Constrained Phase Noise Estimation in OFDM Using Scattered Pilots Without Decision Feedback

Pramod Mathecken, Taneli Riihonen, *Member, IEEE*, Stefan Werner, *Senior Member, IEEE*, and Risto Wichman

***Abstract*—In this paper, we consider an OFDM radio link corrupted by oscillator phase noise in the receiver, namely the problem of estimating and compensating for the impairment. To lessen the computational burden and delay incurred onto the receiver, we estimate phase noise using only scattered pilot subcarriers, i.e., no tentative symbol decisions are used in obtaining and improving the phase noise estimate. In particular, the phase noise estimation problem is posed as an unconstrained optimization problem whose minimizer suffers from the so-called *amplitude and phase estimation error*. These errors arise due to receiver noise, estimation from limited scattered pilot subcarriers and estimation using a dimensionality reduction model. It is empirically shown that, at high signal-to-noise-ratios, the phase estimation error is small. To reduce the amplitude estimation error, we restrict the minimizer to be drawn from the so-called *phase noise geometry* set when minimizing the cost function. The resulting optimization problem is a non-convex program. However, using the *S-procedure for quadratic equalities*, we show that the optimal solution can be obtained by solving the convex dual problem. We also consider a less complex heuristic scheme that achieves the same objective of restricting the minimizer to the phase noise geometry set. Through simulations, we demonstrate improved coded bit-error-rate and phase noise estimation error performance when enforcing the phase noise geometry. For example, at high signal-to-noise-ratios, the probability density function of the phase noise estimation error exhibits *thinner tails* which results in lower bit-error-rate.**

I. Introduction

In this paper, we focus on the phase noise problem in orthogonal frequency division multiplexing (OFDM) which falls in the category of RF-impairments. It is well known that the OFDM waveform is sensitive to RF-impairments which also include power amplifier non-linearities, IQ-imbalance and jitter noise [1]. Phase noise refers to random fluctuations in the phase of the carrier signal that is used for transmission and reception of the baseband information-bearing signal. It arises due to imperfections in the local oscillators that generate the carrier signals. These imperfections exist, simply, due to the inherent physical nature of these devices but, however, it can be controlled by judicious choice of oscillator design [2].

Manuscript received May 17, 2016; revised September 5, 2016 and December 18, 2016; accepted December 30, 2016. The associate editor in charge of handling and coordination of the manuscript was Prof. Yongming Huang. The work of S. Werner was supported in part by the Academy of Finland under Grant 296849.

P. Mathecken, T. Riihonen and R. Wichman are with Aalto University School of Electrical Engineering, Department of Signal Processing and Acoustics, P.O. Box 13000, FI-00076 Aalto, Finland (Email: {pramod.mathecken, taneli.riihonen, stefan.werner, risto.wichman}@aalto.fi). S. Werner is with the Department of Electronic Systems, Norwegian University of Science and Technology, Trondheim NO-7491, Norway (e-mail: stefan.werner@ntnu.no).

In the area of performance analysis, plethora of studies demonstrate a performance drop for an OFDM system corrupted by phase noise [3]–[8]. The performance metrics typically used are: signal-to-noise-plus-interference-ratio (SINR), bit-error-rate (BER) and channel capacity. The trade-off is typically between the OFDM subcarrier spacing and 3-dB bandwidth of oscillator power spectral density (PSD) which in turn can be related to the oscillator topology and circuit parameters [9]. A small ratio of subcarrier spacing and 3-dB PSD bandwidth results in lower SINR, lower capacity and higher BER. These performance studies were indeed extended to include other kinds of RF-impairments which are mainly IQ-imbalance, power amplifier non-linearities and jitter noise [10]. Numerous algorithms are available that remove phase noise from the received OFDM signal. These methods typically require knowledge of the channel. Some of the state-of-the-art methods on channel estimation in the presence of phase noise can be found in [11]–[16].

The phase noise estimation algorithms can be broadly classified into three types: decision-feedback-based schemes also known as decision-directed algorithms [14], [16]–[21]; pilot-based schemes that use the scattered pilot structure provided in LTE [12], [22], [23]; and, finally, blind estimation schemes [24], [25]. Decision-feedback schemes estimate phase noise using tentative decisions on the transmitted symbols. Using the obtained estimate, phase noise is removed and new decisions on the transmitted symbols are taken which are again used to refine the phase noise estimate. The process is iterated over a certain number of times, thus, resulting in a feedback loop. Because of this iteration procedure, these schemes can impose a significant computational burden onto the receiver. The primary goal in blind estimation schemes is to jointly estimate phase noise and transmitted symbols. These approaches typically use Bayesian filtering methods to jointly estimate the desired parameters [26]. For example, in [25], *variational-inference* is used, while *Monte-Carlo* methods are used in [24]. These methods, although statistically optimal, are computationally intensive and may not be suitable in delay-sensitive wireless systems.

Pilot-based schemes that utilize scattered pilot subcarriers are a computationally attractive alternative to decision-feedback and blind estimation schemes. There exists plethora of work where, using scattered pilot subcarriers, only the *common phase error* (CPE) is estimated while the higher-order frequency components of phase noise, also known by *inter-carrier-interference* (ICI), are assumed to be small and, hence, not estimated [27]–[29]. It is well known that, for satisfactory performance, the ICI must also be estimated. To the best of our knowledge, [12], [22] and [23] are the only available works

that, using only scattered pilot subcarriers, estimate both CPE and ICI terms. One of the goals of this paper is to contribute towards scattered pilot-based phase noise estimation schemes that estimate both CPE and ICI with high degree of accuracy.

In this paper, for phase noise estimation, we use two new aspects of phase noise that have been recently discovered: the first is the so-called *phase noise spectral geometry*; and second is a new dimensionality reduction model that preserves this geometry when moving from lower to higher dimensional spaces. These two aspects of phase noise were originally proposed in [17], however, used in developing a decision-feedback phase noise estimation scheme which has high complexity. We build upon these ideas to develop a novel scattered pilot-based estimation scheme without any decision feedback loop. We show in this work that utilizing the phase noise spectral geometry in conjunction with this new dimensionality reduction model improves the estimation performance and, hence, the BER.

The main contributions of this paper are as follows:

- As our starting point, we use the least-squares (LS) approach of [23] to estimate the desired phase noise spectral vector using scattered pilot subcarriers. We show that the minimizer of the resulting unconstrained optimizaton problem suffers from *amplitude and phase estimation errors* which arises due to receiver noise, estimation from limited scattered pilot subcarriers and estimation using a dimensionality reduction model. We empirically show that, at high SNRs, the phase estimation error is small and the critical factor is the amplitude estimation error.
- To eliminate the amplitude estimation error, we impose the phase noise geometry as constraints when minimizing our cost function. The resulting optimization problem is a non-convex program, and we show using the so-called *S-procedure* that the optimization problem can be solved equivalently using the convex dual problem. We also present a heuristic scheme with reduced computational complexity that achieves the same objective of enforcing the estimate to satisfy the phase noise geometry.
- We provide conditions for the S-procedure to be lossless for generic quadratic equalities. In [17], the authors present the S-procedure for quadratic equalities specific to their problem. In this paper, we build upon the ideas presented in [17] and generalize the S-procedure for generic quadratic equalities. We use the S-procedure to prove optimality of our proposed optimization problem.

The paper is structured as follows: In Section II, we present the OFDM system model impaired by phase noise. This shall serve as the foundation for the rest of the paper. Section III covers two particular aspects: The first aspect summarizes the findings of [17] which are the phase noise spectral geometry and the phase noise geometry-based dimensionality reduction model. The second aspect dwells on the topic of S-procedure for generic quadratic equalities. We use the S-procedure in later sections to prove optimality of the proposed phase noise optimization problem. Section IV presents the proposed scattered pilot-based phase noise estimation schemes. Specifically, two new schemes are proposed with the first being the optimal scheme while the second scheme is heuristic in nature, however, with reduced computational complexity. In Section V, we present numerical results of these schemes.

II. System Model

In an OFDM system, an information symbol vector, denoted by $\mathbf{s} = [s_0 \ s_1 \dots s_{N_c-1}]^{\mathrm{T}}$, is transmitted using N_c orthogonal subcarriers [30]. These subcarriers pass through a frequency-selective channel whose discrete-time impulse response is denoted by $h[n]$. At the receiver side, the signal gets corrupted by the receiver additive noise and phase noise. Assuming sufficient timing synchronization, the received symbol vector is given by

$$\mathbf{r} = \mathbf{V}\mathbf{H}\mathbf{s} + \mathbf{n}, \tag{1}$$

where $\mathbf{H}$ is a diagonal matrix composed of elements $\{H_k\}_{k=0}^{N_c-1}$ which are the discrete Fourier transform (DFT) of $h[n]$, i.e.,

$$H_k = \sum_{n=0}^{N_c-1} h[n] e^{-\jmath(2\pi kn)/N_c}, k = 0, 1, \dots, N_c - 1. \tag{2}$$

The vector $\mathbf{n}$ denotes the additive receiver noise which is Gaussian with diagonal covariance matrix whose diagonal values are equal to σ_n^2. The effect of phase noise is represented by the unitary matrix $\mathbf{V}$ which is row-wise circulant with the first row vector being $\boldsymbol{\delta}^\dagger$ which denotes Hermitian transpose of the column vector $\boldsymbol{\delta}$. The elements of $\boldsymbol{\delta}$ are given by

$$\delta_k = \sum_{n=0}^{N_c-1} \frac{e^{-\jmath\theta[n]}}{N_c} e^{-\jmath(2\pi kn)/N_c}, k = 0, 1 \dots, N_c - 1, \tag{3}$$

where $\theta[n]$ is the receiver phase noise. In this paper, we refer to $\boldsymbol{\delta}$ as the *phase noise spectral vector*.

Ideally, in the absence of phase noise (i.e., when $\theta[n] = 0$) and after using (3), we have $\boldsymbol{\delta} = [1, 0, \dots, 0]^{\mathrm{T}}$ and, hence, $\mathbf{V} = \mathbf{I}_{N_c}$, where $\mathbf{I}_{N_c}$ denotes the $N_c \times N_c$ identity matrix. Equation (1), thus, reduces to $\mathbf{r} = \mathbf{H}\mathbf{s}+\mathbf{n}$ which is the standard OFDM system model with no phase noise. In practice, phase noise is always present which renders $\mathbf{V}$ to constitute non-zero off-diagonal elements.

III. Background: Phase Noise Spectral Geometry, Dimensionality Reduction and S-Procedure

In this section, we dwell on three particular topics which shall be used in later sections to develop phase noise estimation schemes. In Section III-A, we present the geometry of $\boldsymbol{\delta}$, while in Section III-B, we present a new dimensionality reduction model that takes into account this geometrical aspect of $\boldsymbol{\delta}$. Finally in Section III-C, we present the S-procedure for quadratic equalities which shall be used to prove optimality of one of our phase noise estimation schemes. The results in Sections III-A and III-B were originally derived in [17] and, hence, we summarize the main points. The S-procedure for quadratic equalities in Section III-C is a generalization of the approach used in [17] which was limited to quadratic equations specific to their application.

A. Geometry of $\boldsymbol{\delta}$

From (3), we see that $\boldsymbol{\delta}_k$ is the DFT of $\frac{e^{-\jmath\theta[n]}}{N_\mathrm{c}}$ which has *constant-magnitude* time-domain samples. Intuitively, we could expect this time-domain property to manifest in the frequency domain in some equivalent form. This is indeed the case which is easy to show and derived in [17]. Specifically, it is shown that $\boldsymbol{\delta}$ always satisfies

$$\boldsymbol{\delta}^\dagger \mathbf{P}_l \boldsymbol{\delta} = \Lambda_l,\ l = 0, 1 \ldots, N_\mathrm{c} - 1, \tag{4}$$

where Λ_l is the Kronecker delta function, i.e., $\Lambda_0 = 1$ and $\Lambda_l = 0,\ l = 1, 2, \ldots, N_\mathrm{c} - 1$. The matrix $\mathbf{P}_l = (\mathbf{P}_1)^l$ is a permutation matrix defined by the $N_\mathrm{c} \times N_\mathrm{c}$ matrix $\mathbf{P}_1$. The first column of $\mathbf{P}_1$ is given by the $N_\mathrm{c} \times 1$ vector $[0, 1, 0, \ldots, 0]^\mathrm{T}$ and the j-th column is obtained by circularly shifting the vector $j-1$ times to the bottom. For $l = 0$, we get the unit-norm property, where $\mathbf{P}_0 = \mathbf{I}_{N_\mathrm{c}}$.

Equation (1) provides the relation between $\mathbf{r}$ and $\mathbf{s}$ for any OFDM symbol. For different OFDM symbols, we obtain different realizations of the channel matrix $\mathbf{H}$, $\mathbf{V}$ and $\mathbf{n}$. Thus, although $\mathbf{V}$ or $\boldsymbol{\delta}$ vary from one OFDM symbol to another, from (4), we see that $\boldsymbol{\delta}$ is always drawn from a particular set. This is useful from an estimation point of view because we now know *where* to look for $\boldsymbol{\delta}$.

B. Dimensionality Reduction

The effect of phase noise can be *compensated* straightforwardly if we have knowledge of $\boldsymbol{\delta}$. We can then form the matrix $\mathbf{V}$ and perform $\mathbf{V}^\dagger \mathbf{r} = \mathbf{H}\mathbf{s} + \mathbf{V}^\dagger \mathbf{n}$ to remove phase noise (we use the fact that $\mathbf{V}^\dagger \mathbf{V} = \mathbf{I}_{N_\mathrm{c}}$). Thus, the critical task of *estimation* is to obtain this knowledge as accurately as possible using which phase noise can be compensated.

1) The Conventional Model: From the point of view of estimation, estimating the entire vector $\boldsymbol{\delta}$ may not be feasible since the dimensionality of $\boldsymbol{\delta}$, equal to N_c, can be large. For example, in LTE, $N_\mathrm{c} > 100$, and it can be as large as 2048. In practice, system specifications enforce stringent requirements on oscillator performance which effectively result in tolerable and slow-varying phase noise processes. This has the effect of larger concentration of power in the low frequency components represented by the top and bottom components of $\boldsymbol{\delta}$, while the high frequency terms represented by the middle components of $\boldsymbol{\delta}$ constitute only a small fraction of total power. We can, thus, *model* $\boldsymbol{\delta}$ as follows:

$$\boldsymbol{\delta} = \begin{pmatrix} \mathbf{I}_{m\times m} & \mathbf{0}_{k\times k} \\ \mathbf{0}_{N_\mathrm{c}-(m+k)\times m} & \mathbf{0}_{N_\mathrm{c}-(m+k)\times k} \\ \mathbf{0}_{k\times m} & \mathbf{I}_{k\times k} \end{pmatrix} \boldsymbol{\gamma} = \mathbf{L}\boldsymbol{\gamma}, \tag{5}$$

where $\mathbf{0}$ is the matrix of zeros of appropriate dimensions. The matrix $\mathbf{L}$ is of dimension $N_\mathrm{c} \times N$, $N = m + k$, and $\boldsymbol{\gamma}$ comprises of the N low-frequency components. Thus, rather than estimating $\boldsymbol{\delta}$, we estimate the smaller N-dimensional vector $\boldsymbol{\gamma}$ and then use (5) to finally obtain our estimate of $\boldsymbol{\delta}$. Note that from (5), we set the high-frequency components to zero. The model in (5) is commonly used in the literature related to phase noise estimation. We shall also refer to $\mathbf{L}$ as low frequency transformation matrix or LFT. It is useful and practical especially when the phase noise process is slow-varying. Unfortunately, the model of (5) does not guarantee that $\boldsymbol{\delta}$ obtained from (5) will satisfy (4).

2) The Geometry-preserving Model: In [17], a new model relating $\boldsymbol{\delta}$ and $\boldsymbol{\gamma}$ is proposed. This is given as follows: The vector $\boldsymbol{\delta}$ acquires its *properties* from a smaller dimensional phase noise spectral vector $\boldsymbol{\gamma}$ that satisfies the N-dimensional equivalent of (4), i.e.,

$$\boldsymbol{\gamma}^\dagger \tilde{\mathbf{P}}_l \boldsymbol{\gamma} = \tilde{\Lambda}_l,\ l = 0, 1, \ldots, N-1, \tag{6}$$

where $\tilde{\mathbf{P}}_l$ and $\tilde{\Lambda}_l$ are the N-dimensional equivalents of $\mathbf{P}_l$ and Λ_l, respectively. The vectors $\boldsymbol{\delta}$ and $\boldsymbol{\gamma}$ are linearly related as

$$\boldsymbol{\delta} = \mathbf{T}\boldsymbol{\gamma}, \tag{7}$$

where the $N_\mathrm{c} \times N$ matrix $\mathbf{T}$ is of the form

$$\mathbf{T} = \mathbf{F}\tilde{\mathbf{T}}\tilde{\mathbf{F}}^\dagger, \tag{8}$$

where the respective $\tilde{\mathbf{F}}$ and $\mathbf{F}$ are the $N \times N$ and $N_\mathrm{c} \times N_\mathrm{c}$ DFT matrices and the columns $\tilde{\mathbf{t}}_i$ of the $N_\mathrm{c} \times N$ matrix $\tilde{\mathbf{T}}$ must satisfy, for all $l = 1, 2, \ldots, N_\mathrm{c} - 1$,

$$\tilde{\mathbf{T}}^\dagger \tilde{\mathbf{T}} = \tilde{\mathbf{I}},\ \tilde{\mathbf{t}}_i^\dagger \mathbf{D}_l \tilde{\mathbf{t}}_j = 0 \text{ for } i \neq j,\ \sum_{i=0}^{N-1} \tilde{\mathbf{t}}_i^\dagger \mathbf{D}_l \tilde{\mathbf{t}}_i = 0, \tag{9}$$

where the diagonal $\mathbf{D}_l = \mathbf{F}^\dagger \mathbf{P}_l \mathbf{F}$. In comparison with the conventional model of (5), the geometrical model imposes restrictions on $\boldsymbol{\gamma}$ and the transformation matrix $\mathbf{T}$. The role of $\mathbf{T}$ is to preserve the phase noise geometry when moving from lower to higher dimensional spaces. Because of the geometry preserving nature of $\mathbf{T}$, we shall refer to it as the *phase noise geometry preserving transformation* or PPT. In reality, many possible choices of PPT exists and in the following paragraph, we provide one such example that we shall later use.

a) Piecewise constant PPT (PC-PPT): The transformation $\boldsymbol{\delta} = \mathbf{F}\tilde{\mathbf{T}}\tilde{\mathbf{F}}^\dagger\boldsymbol{\gamma}$ can be interpreted as follows: $\tilde{\mathbf{F}}^\dagger\boldsymbol{\gamma}$ is a N-dimensional time-domain vector which is interpolated (by $\tilde{\mathbf{T}}$) to a higher dimensional vector and then transformed to the Fourier domain. Such an interpretation is valid for phase noise since, in general, it is a low-pass process. One of the simplest interpolators is to simply repeat the elements of the time-domain vector, i.e.,

$$\tilde{\mathbf{T}}_\mathrm{pc} = \sqrt{\frac{N_\mathrm{c}}{N}} \begin{pmatrix} \mathbf{1}_{\frac{N_\mathrm{c}}{N}} & \mathbf{0} & \ldots & \mathbf{0} \\ \mathbf{0} & \mathbf{1}_{\frac{N_\mathrm{c}}{N}} & \ddots & \vdots \\ \vdots & \ddots & \ddots & \vdots \\ \mathbf{0} & \ldots & \mathbf{0} & \mathbf{1}_{\frac{N_\mathrm{c}}{N}} \end{pmatrix}, \tag{10}$$

where $\mathbf{1}_{\frac{N_\mathrm{c}}{N}}$ is an $\frac{N_\mathrm{c}}{N} \times 1$ vector of ones and $\mathbf{0}$ is the vector with elements equal to zero. We assume without loss of generality that $\frac{N_\mathrm{c}}{N}$ is even. It can be easily verified that $\tilde{\mathbf{T}}_\mathrm{pc}$ satisfies the conditions of (9) and, hence, $\mathbf{T}_\mathrm{pc} = \mathbf{F}\tilde{\mathbf{T}}_\mathrm{pc}\tilde{\mathbf{F}}^\dagger$ is a PPT.

C. S-procedure for Quadratic Equalities

The S-procedure is a method of replacing a set of quadratic inequalities or equalities with a *linear matrix inequality* (LMI). It is typically used when solving primal and dual optimization problems [31]. In this paper, we concern ourselves with

only quadratic equalities. A good overview of the topic for quadratic inequalities can be found in [32].

Consider the following quadratic forms:

$$q_l(\mathbf{x}) = \mathbf{x}^\dagger \begin{pmatrix} \mathbf{A}_l & \mathbf{d}_l \\ \mathbf{d}_l^\dagger & c_l \end{pmatrix} \mathbf{x}, l = 0, 1, \ldots, L-1, \quad (11)$$

where $\mathbf{x} \in \mathcal{C}^{N+1}$. Define the sets:

$$\mathcal{Q} = \left\{ \Big(q_0(\mathbf{x}), q_1(\mathbf{x}), \ldots, q_{L-1}(\mathbf{x}) \Big)^{\mathrm{T}} : \mathbf{x} \in \mathcal{C}^{N+1} \right\}, \quad (12)$$

$$\mathcal{N} = \left\{ \left(g, \mathbf{0}_{L-1}^{\mathrm{T}} \right)^{\mathrm{T}} \text{ s.t } g < 0 \right\}, \quad (13)$$

where $\mathbf{0}_{L-1}$ is a $L-1 \times 1$ vector of zeros. Now consider the following two statements:

- S1: $q_0(\mathbf{x}) \geq 0$ whenever $q_l(\mathbf{x}) = 0$ for all $l > 0$. This is equivalent to $\mathcal{Q} \cap \mathcal{N} = \emptyset$, where $\cap$ denotes intersection and $\emptyset$ denotes the empty set.
- S2: There exists constants $\rho_l, l = 1, 2, \ldots, L-1$ such that

$$\tilde{\mathbf{A}} = \begin{pmatrix} \mathbf{A}_0 + \sum_{l=1}^{L-1} \rho_l \mathbf{A}_l & \mathbf{d}_0 + \sum_{l=1}^{L-1} \rho_l \mathbf{d}_l \\ (\mathbf{d}_0 + \sum_{l=1}^{L-1} \rho_l \mathbf{d}_l)^\dagger & c_0 + \sum_{l=1}^{L-1} \rho_l c_l \end{pmatrix} \succeq 0. \quad (14)$$

We say that the S-procedure is lossless if the statements S1 and S2 are equivalent, i.e., S1 implies S2 and S2 implies S1. We now have the following Lemma:

Lemma 1. *S2 always implies S1.*

Proof: S2 implies that, for all $\mathbf{x} \in \mathcal{C}^{N+1}$, $\mathbf{x}^\dagger \tilde{\mathbf{A}} \mathbf{x} \geq 0$ and after using the expression of $\tilde{\mathbf{A}}$,

$$q_0(\mathbf{x}) + \sum_{l=1}^{L-1} \rho_l q_l(\mathbf{x}) \geq 0 \quad (15)$$

$$\boldsymbol{\rho}^{\mathrm{T}} \mathbf{y} \geq 0, \text{for } \mathbf{y} \in \mathcal{Q}, \quad (16)$$

where $\boldsymbol{\rho} = [1, \rho_1, \rho_2, \ldots, \rho_{L-1}]^{\mathrm{T}}$. For such a $\boldsymbol{\rho}$, we also have

$$\boldsymbol{\rho}^{\mathrm{T}} \mathbf{y} = g < 0, \text{for } \mathbf{y} \in \mathcal{N}, \quad (17)$$

which results from the definition of $\mathcal{N}$. Thus, from (17) and (16), we see that $\mathcal{Q} \cap \mathcal{N} = \emptyset$ which is equivalent to S1. ■

Unfortunately, S1 does not necessarily imply S2, and only depending upon the type of the set $\mathcal{Q}$ it may imply S2. By imposing a certain type of structure on $\mathcal{Q}$, the implication of S1 to S2 can be achieved. The following *regularity condition* imposes such a structure on $\mathcal{Q}$. First, define the set

$$\tilde{\mathcal{Q}} = \left\{ \mathbf{q}(\mathbf{x}) = \Big(q_1(\mathbf{x}), q_2(\mathbf{x}), \ldots, q_{L-1}(\mathbf{x}) \Big)^{\mathrm{T}} : \mathbf{x} \in \mathcal{C}^{N+1} \right\}. \quad (18)$$

We form a matrix

$$\mathbf{Q} = \left[\mathbf{q}(\mathbf{x}_1)\ \mathbf{q}(\mathbf{x}_2)\ \mathbf{q}(\mathbf{x}_3) \ldots \mathbf{q}(\mathbf{x}_M) \right], \quad (19)$$

for some $\{\mathbf{x}_i\}_{i=1}^M$.

Regularity condition 1. *There exists vectors* $\{\mathbf{x}_i\}_{i=1}^M \neq \mathbf{0}$, *where* $M > L-1$, *and constants* $\{p_i\}_{i=1}^M > 0$ *such that*

$$\mathbf{rank}\Big(\mathbf{Q}\Big) = L - 1, \quad (20)$$

$$\sum_{i=1}^{M} p_i \mathbf{q}(\mathbf{x}_i) = \mathbf{0}. \quad (21)$$

***Remark* 1.** *The regularity condition implies that there does not exist any hyperplane passing through the origin such that all points* $\{\mathbf{q}(\mathbf{x}_i)\}_{i=1}^M$ *lie on one side of the hyperplane. This is seen as follows: For any non-zero* $\tilde{\mathbf{a}} \in \mathcal{R}^{L-1}$, *taking the inner product w.r.t.* $\tilde{\mathbf{a}}$ *on both sides of* (21), *we have* $\sum_{i=1}^M p_i(\tilde{\mathbf{a}}^{\mathrm{T}} \mathbf{q}(\mathbf{x}_i)) = 0$ *which implies that* $\tilde{\mathbf{a}}^{\mathrm{T}} \mathbf{q}(\mathbf{x}_i) \geq 0$ *or* $\tilde{\mathbf{a}}^{\mathrm{T}} \mathbf{q}(\mathbf{x}_i) \leq 0$ *for all* $i = 1, 2, \ldots, M$ *is not possible since* $\{p_i\}_{i=1}^M > 0$. *The special case of* $\tilde{\mathbf{a}}^{\mathrm{T}} \mathbf{q}(\mathbf{x}_i) = 0$ *for all* $i = 1, 2, \ldots, M$ *implies* $\mathbf{rank}\,(\mathbf{Q}) < L-1$ *which contradicts with* (20). *Hence, for any non-zero* $\tilde{\mathbf{a}}$, *we must have*

$$\tilde{\mathbf{a}}^{\mathrm{T}} \mathbf{q}(\mathbf{x}_i) < 0,\ \tilde{\mathbf{a}}^{\mathrm{T}} \mathbf{q}(\mathbf{x}_j) > 0 \text{ for some } i \text{ and } j, i \neq j. \quad (22)$$

***Remark* 2.** *The regularity condition also implies that the conic hull of* $\tilde{\mathcal{Q}}$ *is equal to* $\mathcal{R}^{L-1}$. *This follows from Remark 1.*

We now have the following theorem on the losslessness of the S-procedure.

Theorem 1. *Assume* $\tilde{\mathcal{Q}}$ *satisfies the regularity condition. Let* $\mathrm{cov}\,(\mathcal{Q})$ *denote the convex hull of* $\mathcal{Q}$. *If* $\mathcal{Q} \cap \mathcal{N} = \emptyset$ *implies* $\mathrm{cov}\,(\mathcal{Q}) \cap \mathcal{N} = \emptyset$ *then the S-procedure is lossless.*

Proof: First, we note that $\mathcal{Q} \cap \mathcal{N} = \emptyset$ implies the sets are disjoint. Also, the sets $\mathcal{N}$ are $\mathrm{cov}\,(\mathcal{Q})$ are convex sets. Thus, if $\mathcal{Q} \cap \mathcal{N} = \emptyset$ implies $\mathrm{cov}\,(\mathcal{Q}) \cap \mathcal{N} = \emptyset$ then there exists a hyperplane *passing through the origin* that separates $\mathrm{cov}\,(\mathcal{Q})$ and $\mathcal{N}$ [31], [33], i.e., there exists constants a_l such that

$$\mathbf{a}^T \mathbf{y} \leq 0,\ \mathbf{y} \in \mathcal{N}, \quad (23)$$

$$\mathbf{a}^T \mathbf{y} \geq 0,\ \mathbf{y} \in \mathrm{cov}(\mathcal{Q}), \quad (24)$$

where $\mathbf{a} = [a_0, a_1, \ldots, a_{L-1}]^{\mathrm{T}}$. From (23) and definition of $\mathcal{N}$, we must have $a_0 \geq 0$. Now $a_0 = 0$ is impossible because of the regularity condition assumption. This is seen as follows: First, define the vector $\tilde{\mathbf{a}}$ with components as $\{a_i\}_{i=1}^{L-1}$. Assume $a_0 = 0$ is true. Then at points $[q_0(\mathbf{x}_i)\ \mathbf{q}(\mathbf{x}_i)^{\mathrm{T}}]^{\mathrm{T}} \in \mathrm{cov}(\mathcal{Q})$ with $\{\mathbf{x}_i\}_{i=1}^M$ as defined in the regularity condition, (24) becomes

$$\tilde{\mathbf{a}}^{\mathrm{T}} \mathbf{q}(\mathbf{x}_i) \geq 0, \text{for all } i = 1, 2, \ldots, M. \quad (25)$$

Equation (25) contradicts with (22) of Remark 1 which is satisfied because of the regularity condition assumption. Hence, $a_0 > 0$ is necessary. Hence, for all $\mathbf{x} \in \mathcal{C}^{N+1}$, (24) implies

$$q_0(\mathbf{x}) + \sum_{l=1}^{L-1} \frac{a_l}{a_0} q_1(\mathbf{x}) \geq 0. \quad (26)$$

Writing $\rho_l = \frac{a_l}{a_0}$, and after substituting the expressions of $q_l(\mathbf{x})$ we obtain (14), i.e., S1 implies S2. After using Lemma 1, we have S1 equivalent to S2. ■

IV. Phase Noise Estimation Schemes

In this section, we present scattered pilot-based phase noise estimation schemes that take into account the phase noise spectral geometry. In [23], the authors estimate $e^{-\jmath\theta[n]}$ from scattered pilots using the LS approach. We can equivalently apply the same approach in the frequency domain for estimation of $\boldsymbol{\delta}$. Through error analysis, we show that the derived LS estimator suffers from amplitude and phase estimation errors. We improve the scheme by enforcing the phase noise geometry as constraints when minimizing the LS cost function.

A. Unconstrained LS (ULS) Estimation of [23]

From (1), the desired quantity is the term $\mathbf{Hs}$, where $\mathbf{H}$ is the true channel matrix. What we know are the following: an estimate of $\mathbf{H}$ denoted by $\hat{\mathbf{H}}$; and a subset of elements of $\mathbf{s}$ which are the scattered pilot-subcarriers denoted by the $K \times 1$ vector $\mathbf{s}_\mathrm{p}$. The channel estimate $\hat{\mathbf{H}} = \mathbf{H} + \mathbf{E}_\mathrm{ch}$, where $\mathbf{E}_\mathrm{ch}$ is the channel estimation error. Thus, we have knowledge of

$$\mathbf{w}_\mathrm{p} = \hat{\mathbf{H}}_\mathrm{p}\mathbf{s}_\mathrm{p}, \tag{27}$$

where the $K \times K$ diagonal matrix $\hat{\mathbf{H}}_\mathrm{p} = \mathbf{K}\hat{\mathbf{H}}\mathbf{K}^\dagger$ contains as elements the diagonal values of $\hat{\mathbf{H}}$ corresponding to the pilot-subcarrier indices. This selection of diagonal values from $\hat{\mathbf{H}}$ is performed using the $K \times N_\mathrm{c}$ matrix $\mathbf{K}$, where its rows are orthogonal and given by the unit-vectors $\mathbf{e}_j^\mathrm{T} = [0, \ldots, 0, 1, 0, \ldots, 0], j \in \{1, 2, \ldots, N_\mathrm{c}\}$. The choice of $\mathbf{e}_j$ determines the pilot-subcarrier indices used.

Let $\hat{\mathbf{V}}$ denote our estimate of the $\mathbf{V}$ in (1). Since $\mathbf{V}$ is unitary circulant with row vector $\boldsymbol{\delta}^\dagger$, we also assume $\hat{\mathbf{V}}$ to be unitary and row-wise circulant with the row vector $\hat{\boldsymbol{\delta}}^\dagger$, where $\hat{\boldsymbol{\delta}}$ denotes our estimate of $\boldsymbol{\delta}$. Then the value (or estimate) of $\mathbf{w}_\mathrm{p}$ that is observed from $\mathbf{r}$ of (1) is given by

$$\hat{\mathbf{w}}_\mathrm{p} = \mathbf{K}\hat{\mathbf{V}}^\dagger\mathbf{r} = \mathbf{K}\mathbf{R}\hat{\boldsymbol{\delta}}, \tag{28}$$

where $\mathbf{R}$ is column-wise circulant with first column vector $\mathbf{r}$. The j-th column of $\mathbf{R}$ is obtained by circularly shifting $\mathbf{r}$ $j-1$ times to the bottom. In the above equation, we have rewritten $\hat{\mathbf{V}}^\dagger\mathbf{r}$ as $\mathbf{R}\hat{\boldsymbol{\delta}}$ since $\hat{\mathbf{V}}^\dagger$ is unitary circulant with $\hat{\boldsymbol{\delta}}$. The vector $\hat{\boldsymbol{\delta}}$ can now be estimated by minimizing the LS error between $\hat{\mathbf{w}}_\mathrm{p}$ and the known $\mathbf{w}_\mathrm{p}$ of (27) which is given by

$$\mathcal{J}(\hat{\boldsymbol{\delta}}) = \|\mathbf{K}\mathbf{R}\hat{\boldsymbol{\delta}} - \mathbf{w}_\mathrm{p}\|_2^2. \tag{29}$$

The minimizer to (29) is not unique since the number of unknowns equal to N_c is greater than the number of equations equal to K. A unique solution can be obtained by reducing the dimensionality of $\hat{\boldsymbol{\delta}}$. To do so, we use the dimensionality reduction model of Section III-B, where we model $\hat{\boldsymbol{\delta}}$ as

$$\hat{\boldsymbol{\delta}} = \mathbf{T}\hat{\boldsymbol{\gamma}}, \tag{30}$$

where $\mathbf{T}$ is a $N_\mathrm{c} \times N$ known transformation matrix with N orthogonal basis vectors and $\hat{\boldsymbol{\gamma}}$ is the unknown $N \times 1$ vector with $N \ll N_\mathrm{c}$. To see the relation between (30) and our desired $\boldsymbol{\delta}$, let us represent $\boldsymbol{\delta}$ using a basis set $\mathbf{B}$ as follows

$$\boldsymbol{\delta} = \mathbf{B}\boldsymbol{\alpha} = \mathbf{T}\boldsymbol{\gamma} + \mathbf{U}\boldsymbol{\beta}, \tag{31}$$

where $N_\mathrm{c} \times N_\mathrm{c}$ matrix $\mathbf{B} = [\mathbf{T} \;\; \mathbf{U}]$ with $\mathbf{U}$ of dimension $N_\mathrm{c} \times N_\mathrm{c} - N$ and $\mathbf{T}$, as defined below (30), are disjoint subspaces with respect to each other. The $N_\mathrm{c} \times 1$ vector $\boldsymbol{\alpha} = \begin{bmatrix}\boldsymbol{\gamma}^\mathrm{T} & \boldsymbol{\beta}^\mathrm{T}\end{bmatrix}^\mathrm{T}$ with $\boldsymbol{\gamma}$ and $\boldsymbol{\beta}$ of dimension $N \times 1$ and $N_\mathrm{c} - N \times 1$, respectively. The first term in (31) represents that part of $\boldsymbol{\delta}$ that lies in the subspace spanned by the columns of $\mathbf{T}$, while $\mathbf{U}\boldsymbol{\beta}$ represents the part that lies in the subspace spanned by columns of $\mathbf{U}$. Comparing (31) with (30), we see that using (30), we only estimate the first term in (31), where $\hat{\boldsymbol{\gamma}}$ represents our estimate of $\boldsymbol{\gamma}$. The second term in (31) is not estimated using the model in (30). The estimator in (30) is a good estimate when most of the power of $\boldsymbol{\delta}$ is in the subspace spanned by the basis vectors of $\mathbf{T}$. For example, for slow-varying phase noise processes, most of the power of $\boldsymbol{\delta}$ is in its top and bottom components which is captured using the basis set of the matrix $\mathbf{L}$ of (5). Thus, setting $\mathbf{T} = \mathbf{L}$ of (5) ensures that most of the power of $\boldsymbol{\delta}$ is in the first term of (31). Another example is setting $\mathbf{T} = \mathbf{T}_\mathrm{pc}$ of (10) which also spans a subspace that captures slow-varying signals.

Substituting (30) in (29), we have

$$\mathcal{J}(\hat{\boldsymbol{\gamma}}) = \|\mathbf{K}\mathbf{R}\mathbf{T}\hat{\boldsymbol{\gamma}} - \mathbf{w}_\mathrm{p}\|_2^2 \tag{32}$$

$$= \hat{\boldsymbol{\gamma}}^\dagger\mathbf{M}\hat{\boldsymbol{\gamma}} - \hat{\boldsymbol{\gamma}}^\dagger\mathbf{b} - \mathbf{b}^\dagger\hat{\boldsymbol{\gamma}} + \mathbf{b}^\dagger\mathbf{b}, \tag{33}$$

where $\mathbf{M} = \mathbf{T}^\dagger\mathbf{R}^\dagger\mathbf{K}^\dagger\mathbf{K}\mathbf{R}\mathbf{T}$ and $\mathbf{b} = \mathbf{T}^\dagger\mathbf{R}^\dagger\mathbf{K}^\dagger\mathbf{w}_\mathrm{p}$. The minimizer to the above cost function is given by

$$\hat{\boldsymbol{\gamma}} = \mathbf{M}^{-1}\mathbf{b}, \tag{34}$$

and, after using (30), the LS estimate of $\boldsymbol{\delta}$ is given by

$$\hat{\boldsymbol{\delta}}_\mathrm{ls} = \mathbf{T}\mathbf{M}^{-1}\mathbf{b}. \tag{35}$$

We now briefly comment on the effect of channel estimation error on the LS phase noise estimate. Using (27) in $\mathbf{b}$ and the expressions for $\hat{\mathbf{H}}_\mathrm{p}$ and $\hat{\mathbf{H}}$, (35) is expanded as

$$\hat{\boldsymbol{\delta}}_\mathrm{ls} = \hat{\boldsymbol{\delta}}_\mathrm{lsp} + \mathbf{e}_\mathrm{ch}, \tag{36}$$

where $\hat{\boldsymbol{\delta}}_\mathrm{lsp} = \mathbf{T}\mathbf{M}^{-1}\mathbf{T}^\dagger\mathbf{R}^\dagger\mathbf{K}^\dagger\mathbf{K}\mathbf{H}\mathbf{K}^\dagger\mathbf{s}_\mathrm{p}$ represents the LS phase noise estimate with perfect channel knowledge, while the second term $\mathbf{e}_\mathrm{ch} = \mathbf{T}\mathbf{M}^{-1}\mathbf{T}^\dagger\mathbf{R}^\dagger\mathbf{K}^\dagger\mathbf{K}\mathbf{E}_\mathrm{ch}\mathbf{K}^\dagger\mathbf{s}_\mathrm{p}$ represents the error arising due to the channel estimation error. Thus, we see that an accurate LS phase noise estimate requires an accurate channel estimate. Numerous and efficient channel estimation algorithms are available in the general literature which ensure that $\mathbf{e}_\mathrm{ch}$ is small. We refer the reader to [11]–[16] for some of the state-of-the-art methods on channel estimation. In this paper, we use the channel estimator of [12]. To see how well the channel estimator of [12] performs, in Fig. 1, we plot the average ratio of the power of $\mathbf{e}_\mathrm{ch}$ and power of $\hat{\boldsymbol{\delta}}_\mathrm{lsp}$ as a function of SNR. As can be seen from the figure, the power of $\mathbf{e}_\mathrm{ch}$ is very small compared to $\hat{\boldsymbol{\delta}}_\mathrm{lsp}$ even at low SNRs, thereby, ensuring that $\hat{\boldsymbol{\delta}}_\mathrm{ls}$ is very close to its ideal value of $\hat{\boldsymbol{\delta}}_\mathrm{lsp}$.

1) Error Analysis: In this subsection, we shall see the how the LS estimate of (35) is affected by: dimensionality reduction represented by $\mathbf{T}$; limited scattered-pilot knowledge represented by $\mathbf{K}$; and by receiver noise which is embedded in $\mathbf{R}$. The overall effect is introduction of amplitude and phase estimation errors in the LS estimate.

First, we observe that the circulant matrix $\mathbf{R}$ is given by

$$\mathbf{R} = \mathbf{F}\,\mathrm{diag}\left(\mathbf{F}^\dagger\mathbf{r}\right)\mathbf{F}^\dagger \tag{37}$$

$$= \mathbf{F}\,\mathrm{diag}\left(\mathbf{E}_\theta\mathbf{F}^\dagger\mathbf{w} + \mathbf{F}^\dagger\mathbf{n}\right)\mathbf{F}^\dagger \tag{38}$$

$$= \mathbf{F}\left(\mathbf{E}_\theta\mathbf{E}_\mathrm{w} + \mathbf{E}_\mathrm{n}\right)\mathbf{F}^\dagger \tag{39}$$

$$= \mathbf{F}\mathbf{E}_\theta\mathbf{E}_\mathrm{w}\left(\mathbf{I}_{N_\mathrm{c}} + \mathbf{E}_\theta^{-1}\mathbf{E}_\mathrm{w}^{-1}\mathbf{E}_\mathrm{n}\right)\mathbf{F}^\dagger \tag{40}$$

$$= \mathbf{F}\mathbf{E}_\theta\mathbf{E}_\mathrm{w}\mathbf{E}_\mathrm{snr}\mathbf{F}^\dagger, \tag{41}$$

where $\mathrm{diag}\,(\mathbf{x})$ is a diagonal matrix with elements of the vector $\mathbf{x}$ as diagonal values. In (37), we substitute (1) and use $\mathbf{V} = \mathbf{F}\mathbf{E}_\theta\mathbf{F}^\dagger$ to arrive at (38). The diagonal values of the diagonal matrix $\mathbf{E}_\theta$ are $e^{\jmath\theta[i]}, i = 1, \ldots, N_\mathrm{c} - 1$. We denote as $\mathbf{E}_\mathrm{w} = \mathrm{diag}\left(\mathbf{F}^\dagger\mathbf{w}\right)$, $\mathbf{E}_\mathrm{n} = \mathrm{diag}\left(\mathbf{F}^\dagger\mathbf{n}\right)$ and

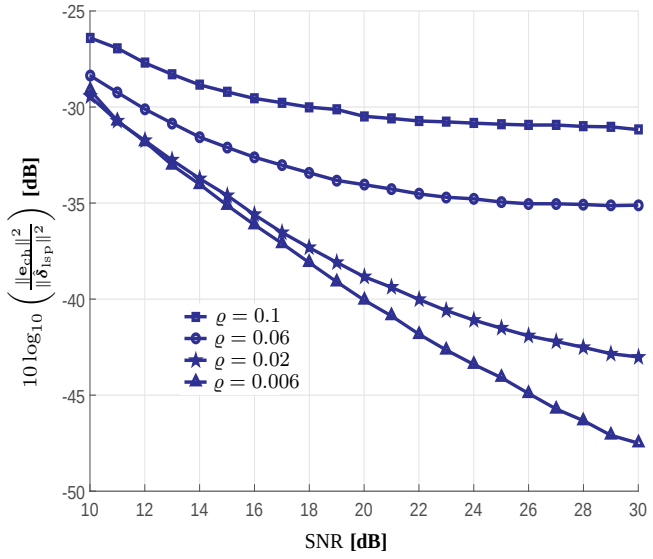

Fig. 1. Effect of channel estimation error on LS estimate of (36). The channel estimator of [12] is used, as an example, for channel estimation. The quantity $\varrho = \frac{f_{3\rm dB}}{f_{\rm sub}}$, where $f_{3\rm dB}$ is the phase noise 3-dB bandwidth and $f_{\rm sub}$ is the OFDM subcarrier spacing. Low and large values of ϱ indicate, respectively, slow-varying and fast-varying processes with respect to the OFDM symbol duration.

$\mathbf{E}_{\rm snr} = \mathbf{I}_{N_{\rm c}} + \mathbf{E}_\theta^{-1}\mathbf{E}_{\rm w}^{-1}\mathbf{E}_{\rm n}$ which captures in some sense the SNR. Using (41) in the expressions for $\mathbf{M}$ and $\mathbf{b}$ while making use of the representation of $\mathbf{T}$ in (8), we can re-write (35) as

$$\hat{\boldsymbol{\delta}}_{\rm ls} = \mathbf{F}\tilde{\mathbf{T}}\left(\tilde{\mathbf{T}}^\dagger\mathbf{E}_{\rm w}^\dagger\mathbf{E}_{\rm snr}^\dagger\mathbf{P}_{\rm r}\mathbf{E}_{\rm snr}\mathbf{E}_{\rm w}\tilde{\mathbf{T}}\right)^{-1}\tilde{\mathbf{T}}^\dagger\mathbf{E}_{\rm w}^\dagger\mathbf{E}_{\rm snr}^\dagger\mathbf{E}_\theta^\dagger\mathbf{F}^\dagger\mathbf{K}^\dagger\mathbf{w}_{\rm p}, \tag{42}$$

where the projection matrix $\mathbf{P}_{\rm r} = \mathbf{E}_\theta^\dagger\mathbf{F}^\dagger\mathbf{K}^\dagger\mathbf{K}\mathbf{F}\mathbf{E}_\theta$. Writing as $\mathbf{E}_{\rm p} = {\rm diag}(\mathbf{F}^\dagger\mathbf{K}^\dagger\mathbf{w}_{\rm p})$ in (42) and using the fact that the diagonal values of $\mathbf{E}_\theta^\dagger$ take the form $e^{-\jmath\theta[i]}$, we finally obtain

$$\hat{\boldsymbol{\delta}}_{\rm ls} = \mathbf{F}\mathbf{C}\mathbf{F}^\dagger\boldsymbol{\delta}, \tag{43}$$

where the $N_{\rm c}\times N_{\rm c}$ matrix $\mathbf{C}$ is given by

$$\mathbf{C} = \tilde{\mathbf{T}}\left(\tilde{\mathbf{T}}^\dagger\mathbf{E}_{\rm w}^\dagger\mathbf{E}_{\rm snr}^\dagger\mathbf{P}_{\rm r}\mathbf{E}_{\rm snr}\mathbf{E}_{\rm w}\tilde{\mathbf{T}}\right)^{-1}\tilde{\mathbf{T}}^\dagger\mathbf{E}_{\rm w}^\dagger\mathbf{E}_{\rm snr}^\dagger\mathbf{E}_{\rm p}. \tag{44}$$

In the ideal case, we would like $\mathbf{C} = \mathbf{I}_{N_{\rm c}}$ which would render complete knowledge of $\boldsymbol{\delta}$. However, the following reasons prevent $\mathbf{C}$ from being the identity matrix:

- Effect of dimensionality reduction: When $N < N_{\rm c}$ we have, in general, ${\rm rank}\,(\mathbf{T}) = {\rm rank}\left(\tilde{\mathbf{T}}\right) = N$. Thus, when $N \le K$ and for any choice of $\mathbf{K}$, $\mathbf{E}_{\rm w}$ and $\mathbf{E}_{\rm snr}$, we have that ${\rm rank}\,(\mathbf{C}) = N$.
- Effect of receiver noise: This is captured by $\mathbf{E}_{\rm snr}$. For example, in the case when $N = N_{\rm c}$ and $\mathbf{K} = \mathbf{I}_{N_{\rm c}}$, we have $\mathbf{P}_{\rm r} = \mathbf{I}_{N_{\rm c}}$, $\mathbf{E}_{\rm p} = \mathbf{E}_{\rm w}$ and (43) reduces to
$$\hat{\boldsymbol{\delta}}_{\rm ls} = \mathbf{F}\mathbf{E}_{\rm snr}^{-1}\mathbf{F}^\dagger\boldsymbol{\delta}. \tag{45}$$
From the expression of $\mathbf{E}_{\rm snr}$, we observe that in the presence of receiver noise, in general, $\mathbf{E}_{\rm snr}^{-1} \neq \mathbf{I}_{N_{\rm c}}$.
- Effect of scattered-pilots: The quantity K denotes the number of scattered-pilot subcarriers. The LS estimation of the $N\times 1$ vector $\hat{\boldsymbol{\gamma}}$ using K scattered-pilot subcarriers imposes the inequality $N \le K < N_{\rm c}$. This results in ${\rm rank}\,(\mathbf{C}) = N$.

The non-identity nature of $\mathbf{C}$ introduces amplitude and phase estimation errors which is seen as follows: Let c_{ij} denote the (i,j)th element of $\mathbf{C}$ and $\hat{\mathbf{x}}_{\rm ls} = \mathbf{F}^\dagger\hat{\boldsymbol{\delta}}_{\rm ls}$. We then have

$$\hat{\mathbf{x}}_{\rm ls}[i] = \frac{e^{-\jmath\theta[i]}}{N_{\rm c}}\left(\sum_{j=0}^{N_{\rm c}-1} c_{ij}e^{\jmath(\theta[i]-\theta[j])}\right) = \frac{\kappa[i]}{N_{\rm c}}e^{-\jmath(\theta[i]-\omega[i])}, \tag{46}$$

where $\kappa[i] = |\left(\sum_{j=0}^{N_{\rm c}-1} c_{ij}e^{\jmath(\theta[i]-\theta[j])}\right)|$ and $\omega[i] = \arg\left(\sum_{j=0}^{N_{\rm c}-1} c_{ij}e^{\jmath(\theta[i]-\theta[j])}\right)$ is the phase estimation error. The amplitude estimation error is given by $\varepsilon[i] = 1-\kappa[i]$ since ideally $\kappa[i] = 1$. The total estimation error is given by

$$\sum_{i=0}^{N_{\rm c}-1}|\hat{\mathbf{x}}_{\rm ls}[i] - \frac{e^{-\jmath\theta[i]}}{N_{\rm c}}|^2 = \frac{1}{N_{\rm c}^2}\Big[\sum_{i=0}^{N_{\rm c}-1}(\varepsilon[i])^2 + 2\varepsilon[i](1-\cos(\omega[i])) + 2\left(N_{\rm c} - \sum_{i=0}^{N_{\rm c}-1}\cos(\omega[i])\right)\Big]. \tag{47}$$

From (47), we see that the estimation error is more sensitive to $\varepsilon[i]$ than $\omega[i]$. This is because it varies quadratically with $\varepsilon[i]$ and, hence, can grow unbounded, while the variation with $\omega[i]$ is bounded because of the limited range of the cosine function. The estimation error is minimum at the values $\varepsilon[i] = 0$ (implies $\kappa[i] = 1$) and $\omega[i] = 0$. Thus, assuming $\omega[i]$ to be small, one way of improving the estimation error is to ensure $\kappa[i] = 1$ which results in $\varepsilon[i] = 0$. For example, we can normalize the samples of $\hat{\mathbf{x}}_{\rm ls}[i]$ which ensures that $\kappa[i] = 1$. However, this is not the only approach and in the next section, we present an optimal way of ensuring $\kappa[i] = 1$. This approach of improving the estimation error works well only when $\omega[i]$ is small. We show empirically that, at high SNRs, this is indeed the case. Figure 2 shows the empirical probability density funtion (PDF) of ω at SNR values of 30-dB, 20-dB and 10-dB. At 30-dB SNR, we see that, for any choice of $\mathbf{T}$, the PDF is highly concentrated around the value of zero. However, as the SNR value is lowered, the PDF of ω is broadened and spread towards higher values, thereby, increasing the overall estimation error. In conclusion, a phase noise estimation strategy that ensures $\kappa[i] = 1$, while assuming a small $\omega[i]$, will be effective mainly at high SNRs.

2) Computational Complexity: We now briefly discuss the complexity in implementing (35). The major effort is the matrix inversion operation of (34) which, in general, requires $O(N^3)$ operations, where $\mathbf{M}$ is of size $N\times N$. Thus, the total complexity is $N^3 + N_{\rm c}N$, where the matrix multiplication in (35) requires $N_{\rm c}N$ operations.

B. Geometry-Constrained LS (GLS) Estimation

In this section, we present an estimation scheme that eliminates the amplitude estimation error introduced by the matrix $\mathbf{C}$. To do so, we utilize the geometrical model of Section III-B2. We first require that we choose $\mathbf{T}$ to be a PPT. We then enforce (6) as constraints when minimizing $\mathcal{J}(\hat{\boldsymbol{\gamma}})$. After obtaining an optimal estimate of $\boldsymbol{\gamma}$, our estimate of $\boldsymbol{\delta}$,

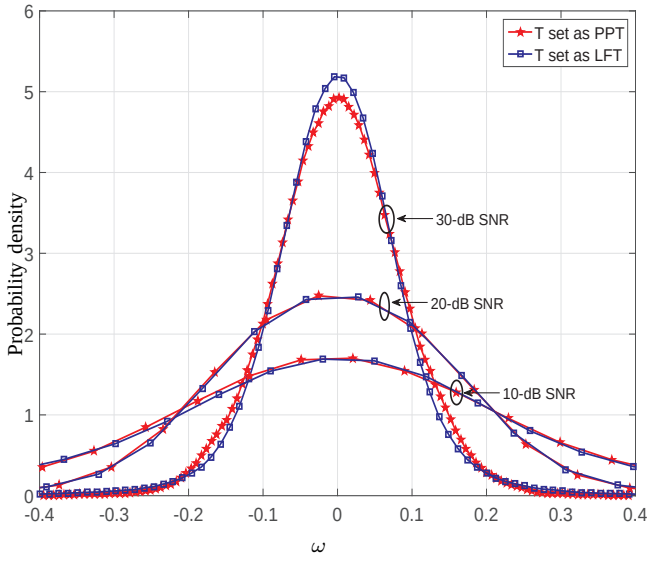

Fig. 2. Empirical PDF of phase estimation error ω at SNR equal to 30, 20 and 10-dB. The PPT and LFT matrix used are $\mathbf{T}_{\rm pc}$ of (10) and $\mathbf{L}$ of (5).

i.e., $\hat{\boldsymbol{\delta}} = \mathbf{T}\hat{\boldsymbol{\gamma}}$ also satisfies (4) (since $\mathbf{T}$ is a PPT), thereby eliminating the amplitude estimation error. The optimization problem in terms of $\hat{\boldsymbol{\gamma}}$ is given by

$$\begin{aligned}(\mathcal{P}): \quad & \text{Minimize } \mathcal{J}(\hat{\boldsymbol{\gamma}}) \\ & \text{s.t } \ \hat{\boldsymbol{\gamma}}^\dagger\hat{\boldsymbol{\gamma}} = 1, \ \hat{\boldsymbol{\gamma}}^\dagger\tilde{\mathbf{P}}_l^{\rm R}\hat{\boldsymbol{\gamma}} = 0, \ \hat{\boldsymbol{\gamma}}^\dagger\tilde{\mathbf{P}}_l^{\rm I}\hat{\boldsymbol{\gamma}} = 0, \\ & \qquad\qquad l = 1, 2, \ldots, \frac{N-1}{2}, \end{aligned} \tag{48}$$

where $\tilde{\mathbf{P}}_l^{\rm R}$ and $\tilde{\mathbf{P}}_l^{\rm I}$ are given by

$$\tilde{\mathbf{P}}_l^{\rm R} = \frac{\tilde{\mathbf{P}}_l + \tilde{\mathbf{P}}_l^\dagger}{2}, \tilde{\mathbf{P}}_l^{\rm I} = \frac{\jmath(\tilde{\mathbf{P}}_l^\dagger - \tilde{\mathbf{P}}_l)}{2}. \tag{49}$$

In (48), we have imposed (6) as constraints, however, for $l > 0$, we have elaborated the equations in terms of its real and imaginary parts, i.e., imposing $\hat{\boldsymbol{\gamma}}^\dagger\tilde{\mathbf{P}}_l\hat{\boldsymbol{\gamma}} = 0$, for $l > 0$, is equivalent to imposing both $\text{Real}\left(\hat{\boldsymbol{\gamma}}^\dagger\tilde{\mathbf{P}}_l\hat{\boldsymbol{\gamma}}\right) = 0$ and $\text{Imag}\left(\hat{\boldsymbol{\gamma}}^\dagger\tilde{\mathbf{P}}_l\hat{\boldsymbol{\gamma}}\right) = 0$, where $\text{Real}\,(x)$ and $\text{Imag}\,(x)$ denote real and imaginary parts of the complex number x. This is done so because $\hat{\boldsymbol{\gamma}}^\dagger\tilde{\mathbf{P}}_l\hat{\boldsymbol{\gamma}}$, for $l > 0$, is a complex function since the eigenvalues of $\tilde{\mathbf{P}}_l$ are complex valued and take the form $\{e^{\jmath\frac{2\pi nl}{N}}\}_{n=0}^{N-1}$. Thus, the constraint $\hat{\boldsymbol{\gamma}}^\dagger\tilde{\mathbf{P}}_l\hat{\boldsymbol{\gamma}} = 0$ can equivalently be expressed by imposing its real and imaginary parts to be zero. The real and imaginary parts of $\hat{\boldsymbol{\gamma}}^\dagger\tilde{\mathbf{P}}_l\hat{\boldsymbol{\gamma}}$ are obtained by noting that $\tilde{\mathbf{P}}_l = \tilde{\mathbf{P}}_l^{\rm R} + \jmath\tilde{\mathbf{P}}_l^{\rm I}$, where $\tilde{\mathbf{P}}_l^{\rm R}$ and $\tilde{\mathbf{P}}_l^{\rm I}$ are defined in (49). Thus,

$$\hat{\boldsymbol{\gamma}}^\dagger\tilde{\mathbf{P}}_l\hat{\boldsymbol{\gamma}} = \hat{\boldsymbol{\gamma}}^\dagger\tilde{\mathbf{P}}_l^{\rm R}\hat{\boldsymbol{\gamma}} + \jmath(\hat{\boldsymbol{\gamma}}^\dagger\tilde{\mathbf{P}}_l^{\rm I}\hat{\boldsymbol{\gamma}}). \tag{50}$$

To avoid confusion, let us point out that $\tilde{\mathbf{P}}_l^{\rm R}$ and $\tilde{\mathbf{P}}_l^{\rm R}$ are actually *not* the real and imaginary parts of $\tilde{\mathbf{P}}_l$ but, rather, it is their quadratic forms that are the real and imaginary parts of the quadratic form of $\tilde{\mathbf{P}}_l$ as seen in (50). The matrices $\tilde{\mathbf{P}}_l^{\rm R}$ and $\tilde{\mathbf{P}}_l^{\rm I}$ are Hermitian with respective eigenvalues of $\{\cos(\frac{2\pi nl}{N})\}_{n=0}^{N-1}$ and $\{\sin(\frac{2\pi nl}{N})\}_{n=0}^{N-1}$. We also point to the reader that only half the number of constraints are enforced in (48). This is because

$$\hat{\boldsymbol{\gamma}}^\dagger\tilde{\mathbf{P}}_l\hat{\boldsymbol{\gamma}} = 0 \text{ implies } \left(\hat{\boldsymbol{\gamma}}^\dagger\tilde{\mathbf{P}}_l\hat{\boldsymbol{\gamma}}\right)^\dagger = 0 \text{ implies } \hat{\boldsymbol{\gamma}}^\dagger\tilde{\mathbf{P}}_{N-l}\hat{\boldsymbol{\gamma}} = 0,$$

where we used the fact that $\tilde{\mathbf{P}}_l^\dagger = \tilde{\mathbf{P}}_{N-l}$. The implication also works in the opposite direction. In (48), we assume that N is odd without any loss in generality.

The optimization problem $(\mathcal{P})$ is typically referred to as the *primal problem*. From (48), we observe that the constraints are *non-convex* in nature. For example, the unit-norm constraint $\hat{\boldsymbol{\gamma}}^\dagger\hat{\boldsymbol{\gamma}} = 1$ describes, mathematically, an N-dimensional sphere, and such an object is a non-convex set. The remaining constraints are also non-convex because the matrices in (49) constitute both positive and negative eigenvalues. The eigenvalues of $\tilde{\mathbf{P}}_l$ are $\{e^{\jmath\frac{2\pi nl}{N}}\}_{n=0}^{N-1}$ and, hence, the eigenvalues of $\tilde{\mathbf{P}}_l^{\rm R}$ and $\tilde{\mathbf{P}}_l^{\rm I}$ are $\{\cos(\frac{2\pi nl}{N})\}_{n=0}^{N-1}$ and $\{\sin(\frac{2\pi nl}{N})\}_{n=0}^{N-1}$, respectively. This non-convexity of the constraints renders $(\mathcal{P})$ to be a *non-convex program*. Most algorithms used in solving non-convex programs yield local optimal solutions.

1) The Convex Dual Problem: A *suboptimal* solution can be obtained by solving the so-called *dual problem* to $(\mathcal{P})$. It can be easily derived and is given by [31]

$$\begin{aligned}(\mathcal{D}): \quad & \text{Maximize } \ \tau \\ & \text{s.t } \begin{pmatrix} \mathbf{M} + \lambda\mathbf{I}_N + \sum_{l=1}^{\frac{N-1}{2}} \alpha_l\tilde{\mathbf{P}}_l^{\rm R} + \beta_l\tilde{\mathbf{P}}_l^{\rm I} & \mathbf{b} \\ \mathbf{b}^\dagger & -\tau - \lambda \end{pmatrix} \succeq 0, \end{aligned} \tag{51}$$

where τ, λ, α_l and β_l are the variables to optimize. In general, the dual problem yields an optimal value different from that of the primal problem (in fact, it is never greater). The dual problem is always a *convex program* which have the property that every local optimal solution is also a global solution. This property eases the search process for algorithms and, in fact, numerous and efficient algorithms exist that solve convex programs in polynomial time. In certain situations, the dual problem can yield the same optimal value as the primal problem, i.e., a difficult non-convex program can be equivalently solved using an easier convex dual program.

Let $\tau^\diamond, \lambda^\diamond, \alpha_l^\diamond$ and $\beta_l^\diamond$ be the minimizer to $(\mathcal{D})$. We obtain our suboptimal estimate of $\boldsymbol{\gamma}$ by solving the Karhush-Kuhn-Tucker (KKT) necessary condition for local optimality of $(\mathcal{P})$ which is given by

$$\left(\mathbf{M} + \lambda^\diamond\mathbf{I}_N + \sum_{l=1}^{\frac{N-1}{2}} \alpha_l^\diamond\tilde{\mathbf{P}}_l^{\rm R} + \beta_l^\diamond\tilde{\mathbf{P}}_l^{\rm I}\right)\hat{\boldsymbol{\gamma}}_{\rm gls} = \mathbf{b} \tag{52}$$

$$\text{implies } \hat{\boldsymbol{\gamma}}_{\rm gls} = \left(\mathbf{M} + \lambda^\diamond\mathbf{I}_N + \sum_{l=1}^{\frac{N-1}{2}} \alpha_l^\diamond\tilde{\mathbf{P}}_l^{\rm R} + \beta_l^\diamond\tilde{\mathbf{P}}_l^{\rm I}\right)^+ \mathbf{b} \tag{53}$$

where $\mathbf{X}^+$ denotes pseudo-inverse of $\mathbf{X}$. The minimizers $\tau^\diamond, \lambda^\diamond, \alpha_l^\diamond$ and $\beta_l^\diamond$ are obtained by solving $(\mathcal{D})$ which is a *semi-definite* program (SDP) [31]. SDPs are convex programs and efficiently solved using interior point algorithms [34]. Standard solvers are available that solve for such programs, for example,

in this paper, we use CVX, a package for solving convex programs [35], [36].

Denote the respective optimal values of $(\mathcal{P})$ and $(\mathcal{D})$ by $p^\star$ and $d^\star$. We say the dual problem yields a *suboptimal* solution whenever $d^\star \leq p^\star$. Such a situation is referred as *weak duality*. When $d^\star = p^\star$, also known by the term *strong duality*, the optimal solution is equivalently achieved by solving the dual problem. In the next paragraph, we dwell on when $d^\star = p^\star$ and show that strong duality holds for the optimization problems $(\mathcal{P})$ and $(\mathcal{D})$.

2) Strong Duality Between $(\mathcal{P})$ and $(\mathcal{D})$: In this section, we shall use the S-procedure described in Section III-C for proving strong duality between the primal and dual problems. For our application, we set the matrices in (11) as follows:

$$\begin{pmatrix} \mathbf{A}_0 & \mathbf{d}_0 \\ \mathbf{d}_0^\dagger & c_0 \end{pmatrix} = \begin{pmatrix} \mathbf{M} & \mathbf{b} \\ \mathbf{b}^\dagger & -\tau \end{pmatrix}, \begin{pmatrix} \mathbf{A}_1 & \mathbf{d}_1 \\ \mathbf{d}_1^\dagger & c_1 \end{pmatrix} = \begin{pmatrix} \mathbf{I}_N & \mathbf{0} \\ \mathbf{0}^\dagger & -1 \end{pmatrix} \tag{54}$$

$$\begin{pmatrix} \mathbf{A}_l & \mathbf{d}_l \\ \mathbf{d}_l^\dagger & c_l \end{pmatrix} = \begin{pmatrix} \mathbf{W}_l & \mathbf{0} \\ \mathbf{0}^\dagger & 0 \end{pmatrix}, l = 2, 3, \ldots, N \tag{55}$$

where $\mathbf{W}_l = \tilde{\mathbf{P}}^{\mathrm{R}}_{l-1}, l = 2, 3, \ldots, \frac{N+1}{2}$ and $\mathbf{W}_l = \tilde{\mathbf{P}}^{\mathrm{I}}_{l-\frac{N+1}{2}}, l = \frac{N+1}{2}+1, \frac{N+1}{2}+2, \ldots, N$. Comparing with (11), we have that $L = N+1$. Define the respective quadratic forms and the set as

$$s_l(\hat{\boldsymbol{\gamma}}) = \begin{pmatrix} \hat{\boldsymbol{\gamma}} \\ -1 \end{pmatrix}^\dagger \begin{pmatrix} \mathbf{A}_l & \mathbf{d}_l \\ \mathbf{d}_l^\dagger & c_l \end{pmatrix} \begin{pmatrix} \hat{\boldsymbol{\gamma}} \\ -1 \end{pmatrix}, l = 0, 1, \ldots, L-1, \tag{56}$$

$$\Pi = \left\{ \left(s_0(\hat{\boldsymbol{\gamma}}), s_1(\hat{\boldsymbol{\gamma}}), \ldots, s_{L-1}(\hat{\boldsymbol{\gamma}}) \right)^{\mathrm{T}} : \hat{\boldsymbol{\gamma}} \in \mathcal{C}^N \right\}. \tag{57}$$

***Remark* 3.** *Let $\mathbf{x} \in \mathcal{C}^{N+1}$. Since $\hat{\boldsymbol{\gamma}} \in \mathcal{C}^N$, we have $\Pi \subseteq \mathcal{Q}$, where the set $\mathcal{Q}$ is defined in* (12)*. The matrices that comprise the quadratic forms q_l are given in* (54) *and* (55)*.*

We are now ready to see how the primal and dual problem can yield the same optimal values. We re-write $(\mathcal{P})$ as

$$\text{Minimize } \mathcal{J}(\hat{\boldsymbol{\gamma}}) \text{ s.t } s_l(\hat{\boldsymbol{\gamma}}) = 0,\ l = 1, \ldots, L-1 \tag{58}$$

which equivalently is expressed as

$$\text{Maximize } \tau$$

$$\text{s.t } \mathcal{J}(\hat{\boldsymbol{\gamma}}) \geq \tau, \text{for all } \hat{\boldsymbol{\gamma}} \text{ satisfying } s_l(\hat{\boldsymbol{\gamma}}) = 0, \tag{59}$$

$$\text{s.t } s_0(\hat{\boldsymbol{\gamma}}) \geq 0, \text{ for all } \hat{\boldsymbol{\gamma}} \text{ satisfying } s_l(\hat{\boldsymbol{\gamma}}) = 0, \tag{60}$$

$$\text{s.t } \Pi \cap \mathcal{N} = \emptyset, \tag{61}$$

where $l = 1, \ldots, L-1$ and the constraint $\mathcal{J}(\hat{\boldsymbol{\gamma}}) \geq \tau$ in (59) is equivalent to $s_0(\hat{\boldsymbol{\gamma}}) \geq 0$ in (60). We obtain the final constraint after observing that the condition $s_0(\hat{\boldsymbol{\gamma}}) \geq 0, s_l(\hat{\boldsymbol{\gamma}}) = 0, l = 1, \ldots, L-1$ is equivalent to (61), where $\mathcal{N}$ is defined in (13). From Remark 3, we have that Π is a subset of $\mathcal{Q}$. Thus, $\mathcal{Q} \cap \mathcal{N} = \emptyset$ is a sufficient condition for $\Pi \cap \mathcal{N} = \emptyset$. We, thus, replace the constraint in (61) to obtain

$$\text{Maximize } \tau, \text{ s.t } \mathcal{Q} \cap \mathcal{N} = \emptyset. \tag{62}$$

If conditions in Theorem 1 are satisfied then, after using (54) and (55), $\mathcal{Q} \cap \mathcal{N} = \emptyset$ is equivalent to the LMI in (51) and, hence, the optimization problem in (62) is nothing but the dual problem of (51). Thus, we see that solving the original primal problem is the same as solving the dual problem and, hence, $d^\star = p^\star$ implying strong duality. In the following proposition, we show $\mathcal{Q}$ indeed satisfies the conditions in Theorem 1.

Proposition 1. *$\mathcal{Q}$ satisfies the conditions of Theorem 1.*

Proof: See Appendix A. ∎

3) Computational Complexity: We now discuss the complexity in obtaining $\hat{\boldsymbol{\gamma}}_{\mathrm{gls}}$ of (53). The estimator requires $\tau^\diamond, \lambda^\diamond, \alpha_l^\diamond$ and $\beta_l^\diamond$ which are obtained by solving the SDP of (51). SDPs are typically solved using interior-point algorithms, and in [34, Chapter 11], the complexity of such methods are discussed. Applying the complexity analysis to the SDP in (51), the resulting complexity is $O(N^{4.5})$. Thus, the overall complexity to obtain $\hat{\boldsymbol{\delta}}_{\mathrm{gls}} = \mathbf{T}\hat{\boldsymbol{\gamma}}_{\mathrm{gls}}$ is $N^{4.5} + N_{\mathrm{c}}N$.

C. Normalization-based LS (NLS) Estimation

One drawback with the GLS scheme is that its complexity of $O(N^{4.5})$ can be high depending upon the value of N. A computationally attractive alternative to the GLS scheme can be obtained by choosing $\mathbf{T}$ to be a PPT and exploiting the time-domain equivalent of (6).

We require that $\hat{\boldsymbol{\gamma}}$ satisfy (6) whose equivalent time-domain manifestation is given by

$$|\mathbf{x}[i]| = \frac{1}{N}, i = 0, 1, \ldots, N-1, \tag{63}$$

where $\mathbf{x} = \tilde{\mathbf{F}}^\dagger \boldsymbol{\gamma}$ and $|c|$ denotes absolute value of the complex number c. Thus, given an estimate of $\boldsymbol{\gamma}$, for example, the LS estimate in (34), we normalize its time-domain samples to have constant magnitude and transform back to the frequency-domain to obtain a refined estimate of $\boldsymbol{\gamma}$. The overall estimation procedure is shown in Table I, where two possible approaches are used depending upon if $\mathbf{T}$ is chosen as a PPT or not. The normalization is performed by the diagonal $N \times N$ matrix $\mathbf{X}_N$ when $\mathbf{T}$ is chosen as a PPT and diagonal $N_{\mathrm{c}} \times N_{\mathrm{c}}$ matrix $\mathbf{X}_{N_{\mathrm{c}}}$ when $\mathbf{T}$ is chosen otherwise. The diagonal values of the normalization matrices are

$$\mathbf{X}_N[i,i] = \frac{1}{N|\tilde{\mathbf{x}}_{\mathrm{ls}}[i]|}, i = 0, 1, \ldots, N-1, \tag{64}$$

$$\mathbf{X}_{N_{\mathrm{c}}}[i,i] = \frac{1}{N_{\mathrm{c}}|\mathbf{x}_{\mathrm{ls}}[i]|}, i = 0, 1, \ldots, N_{\mathrm{c}}-1. \tag{65}$$

In Step 1 of Table I, we obtain the LS estimate which, in general, requires N^3 number of operations. We then transform the LS estimate to the time-domain and normalize the samples to have constant-magnitude. When $\mathbf{T}$ is chosen as a PPT, it suffices to only perform normalization in the N-dimensional space. This is because after normalization, $\tilde{\mathbf{x}}_{\mathrm{nls}}$ (Step 3) satisfies (63) and, hence, $\hat{\boldsymbol{\gamma}}_{\mathrm{nls}}$ (Step 4) satisfies (6). Thus, $\hat{\boldsymbol{\delta}}_{\mathrm{nls}} = \mathbf{T}\hat{\boldsymbol{\gamma}}_{\mathrm{nls}}$ also satisfies the phase noise geometry in the N_{c}-dimensional space when $\mathbf{T}$ is a PPT. The added number of computations is mainly $2N\log(N)$ which correspond to the two N-point DFT operations for moving between time and frequency domain. However, when $\mathbf{T}$ is not a PPT, even after normalization, there is no guarantee that $\hat{\boldsymbol{\delta}}_{\mathrm{nls}}$ will satisfy the phase noise geometry. To ensure that it does satisfy when

TABLE I
NORMALIZATION-BASED LS ESTIMATION.

When $\mathbf{T}$ is a PPT		When $\mathbf{T}$ is not a PPT	
Steps	**Function**	**Steps**	**Function**
1	$\hat{\boldsymbol{\gamma}}_{\rm ls} = \mathbf{M}^{-1}\mathbf{b}$	1	$\hat{\boldsymbol{\gamma}}_{\rm ls} = \mathbf{M}^{-1}\mathbf{b}$
2	$\tilde{\mathbf{x}}_{\rm ls} = \tilde{\mathbf{F}}^{\dagger}\hat{\boldsymbol{\gamma}}_{\rm ls}$	2	$\hat{\boldsymbol{\delta}}_{\rm ls} = \mathbf{T}\hat{\boldsymbol{\gamma}}_{\rm ls}$
3	$\tilde{\mathbf{x}}_{\rm nls} = \mathbf{X}_N\tilde{\mathbf{x}}_{\rm ls}$	3	$\mathbf{x}_{\rm ls} = \mathbf{F}^{\dagger}\hat{\boldsymbol{\delta}}_{\rm ls}$
4	$\hat{\boldsymbol{\gamma}}_{\rm nls} = \tilde{\mathbf{F}}\tilde{\mathbf{x}}_{\rm nls}$	4	$\mathbf{x}_{\rm nls} = \mathbf{X}_{N_{\rm c}}\mathbf{x}_{\rm ls}$
5	$\hat{\boldsymbol{\delta}}_{\rm nls} = \mathbf{T}\hat{\boldsymbol{\gamma}}_{\rm nls}$	5	$\hat{\boldsymbol{\delta}}_{\rm nls} = \mathbf{F}\mathbf{x}_{\rm nls}$
Operations $\approx N^3 + 2N\log(N) + N_{\rm c}N$		Operations $\approx N^3 + 2N_{\rm c}\log(N_{\rm c})$	

$\mathbf{T}$ is not a PPT, the normalization must be done in the $N_{\rm c}$-dimensional space as shown in right half of Table I. This comes at the cost of higher complexity which is two $N_{\rm c}$-point DFT operations.

V. NUMERICAL RESULTS

We now present numerical results of the proposed phase noise estimation schemes and compare them with some of the state-of-the-art scattered pilot-based phase noise estimation schemes. In particular, we compare our proposed GLS and NLS scheme with the ULS scheme of [23] and the CPE-based interpolation schemes of [12] and [22].

The system parameters set for the simulations are as follows: The number of subcarriers $N_{\rm c} = 512$; subcarrier spacing $f_{\rm sub} = 15$ kHz; bandwidth is 7.7 MHz. The percentage of scattered pilot subcarriers is set to 8% and symbol constellation is 16-QAM. The channel is Rayleigh fading with four exponentially decaying taps, and coherence bandwidth is set to 800 kHz. We use a $1/2$-rate convolutional encoder $[133, 171]$ with constraint length of 7. For decoding, we use a soft-decision Viterbi decoder of decoding depth equal to five times the constraint length. Phase noise process used in the simulations is the Wiener process which models well free-running oscillators. We denote $f_{\rm 3dB}$ as the phase noise 3-dB bandwidth, and the quantity $\varrho = \frac{f_{\rm 3dB}}{f_{\rm sub}}$ is a measure of how fast or slow phase noise varies within an OFDM symbol. A low value of ϱ indicates a slow-varying process and a larger value implies a fast-varying one.

The phase noise estimation schemes of this paper require knowledge of the channel. This knowledge is acquired by estimating the channel. In this paper, we use the channel estimator of [12] which is computationally attractive compared to other schemes and at the same time takes into account the effect of phase noise during the estimation process.

A. CPE-based Interpolation Scheme (CIS) of [12] and [22]

We now briefly summarize the interpolation schemes of [12] and [22]. The goal is to develop a non-iterative scheme for phase noise estimation for data OFDM symbols. Such a phase noise estimate is obtained as follows: The CPE of the current and next OFDM symbol are estimated using scattered pilot subcarriers. The average value of phase noise in the current and next OFDM symbol is then obtained by taking the angle of the obtained CPE estimates. The mean phase noise values are then interpolated to obtain the entire phase noise realization between the mid-points of the current and next OFDM symbols. A linear interpolator is used in both [12] and [22]. In fact, it is shown in [12] that for slow-varying phase noise processes, the optimal interpolator, in terms of minimum mean square error, is the linear interpolator. However, for moderate or fast-varying processes, we can expect inferior performance which is verified by the numerical results.

TABLE II
COMPARISON OF COMPUTATIONAL COMPLEXITY

Method	**Complexity Order**
ULS	$N^3 + N_{\rm c}N$
GLS	$N^{4.5} + N_{\rm c}N$
NLS	$N^3 + 2N\log(N) + N_{\rm c}N$
CIS	$K + N_{\rm c} + N_{\rm cp}$

The CIS schemes are simple and computationally very attractive. For example, from [12], we see that the number of operations required is approximately of the order $K + N_{\rm c} + N_{\rm cp}$, where K is the number of scattered-pilot symbols and $N_{\rm cp}$ is the cyclic prefix length. Table II compares the complexity of the CIS scheme with the proposed phase noise estimation schemes. As seen from the table, CIS is the most computationally simplest scheme, however, as we shall see, it has very poor performance.

B. Discussion

Figure 3 shows coded BER performance of the proposed phase noise estimation schemes. The ideal performance that can be achieved is shown by the triangle-marker dashed curve which corresponds to the case of zero phase noise. The squared-marker curve represents the case where only CPE compensation is performed. This method works well only for extremely slow-varying phase noise processes. As seen from the figure, the best performance is achieved by the GLS scheme and is close to the ideal performance. It also outperforms the CIS schemes of [12] and [22] as expected. The GLS scheme constraints the LS estimator to adhere to the phase noise geometry. As seen in the figure, the ULS scheme, which is the unconstrained LS estimator, has an inferior performance compared to its constrained GLS counterpart. The NLS scheme is a suboptimal solution that also achieves the same objective of delivering an estimate that satisfies the phase noise geometry. As expected, the NLS scheme has a better performance compared to ULS.

The BER performance of the phase noise estimation schemes can be explained by examining the PDF of $\|\hat{\boldsymbol{\delta}} - \boldsymbol{\delta}\|^2$, where $\hat{\boldsymbol{\delta}}$ is our estimate of the true value of $\boldsymbol{\delta}$. In Figs. 4a and 4b, we plot the empirical PDF of $\|\hat{\boldsymbol{\delta}} - \boldsymbol{\delta}\|^2$ for SNR of 30-dB and 10-dB, respectively. From Fig. 4a, we see that the GLS scheme exhibits thinner tails in the PDF compared to all other schemes. The thicker tails seen, for example, in the ULS scheme results in a higher BER as verified in Fig. 3 at SNR

equal to 30-dB. In Fig. 4b, at the lower SNR of 10-dB, for all schemes, we see that the PDF of the phase noise estimation error is spread over a large range of values, thereby, resulting in a much higher BER.

A moderate value of $\varrho = 0.02$ was used in the simulation results shown in Figs. 3 and 4. It is of practical interest to see how well the proposed algorithms perform over the practical range of values of ϱ. This is demonstrated in Fig. 5, where we plot the BER as a function of ϱ. A small value of ϱ indicates a slow-varying phase noise process in comparison with the OFDM symbol duration and vice-versa. As expected and verified in the figure, the BER, in general, increases with ϱ. The best performance is obtained by the GLS scheme, however, for low values of ϱ, the CIS scheme is as good as the GLS scheme. However, as the value of ϱ increases, CIS performs the poorest. This is easily seen since the CIS scheme obtains the entire phase noise realization using a linear interpolator. As the value of ϱ increases, the phase noise realization is more fast-varying in nature, and a simple linear interpolator does a poor job of approximation. A similar behavior is seen in Fig. 6, where we plot the mean-square-error (MSE) of $\hat{\boldsymbol{\gamma}}$, i.e., $\mathrm{E}\left[\|\hat{\boldsymbol{\gamma}} - \boldsymbol{\gamma}\|^2\right]$ as a function of ϱ.

We now compare the effect of the transformation matrix $\mathbf{T}$ on the proposed phase noise estimation schemes. Figure 7 shows the average coded-BER for the ULS and NLS schemes with $\mathbf{T}$ set to $\mathbf{T}_{\mathrm{pc}}$ of (10) and with $\mathbf{T} = \mathbf{L}$ of (5). From the figure we see that for $\mathbf{T}$ equal to PPT, the ULS and NLS schemes yield a lower average BER compared to the case when $\mathbf{T}$ is set as LFT, especially at high SNRs. We can again explain this behavior by examining the PDF of $\|\hat{\boldsymbol{\delta}} - \boldsymbol{\delta}\|^2$ which is shown in Fig. 8a, where SNR is set to 30-dB. From the figure, we see that when $\mathbf{T}$ is equal to the LFT of (5), the empirical PDF, of both ULS and NLS, exhibits thicker tails compared to the curves $\mathbf{T}$ equal to PPT. Also plotted in the figure is the GLS scheme. Note that for GLS $\mathbf{T}$ is set to $\mathbf{T}_{\mathrm{pc}}$ of (10). These thicker tails eventually cause higher BER as observed in Fig. 7 at SNR equal to 30-dB. Figure 8b shows the empirical PDF at SNR equal to 10-dB. As can be seen, for any choice of $\mathbf{T}$, the ULS and NLS exhibit similar behavior especially at the tails of the PDF. Thus, we can expect similar BER as evidenced in Fig. 7 at SNR of 10-dB.

The effect of the transformation matrix $\mathbf{T}$ can also be visualized by looking at the estimated phase noise realization. We illustrate this effect, for example, using the ULS scheme. Figures 9a and 9b show, respectively, the estimated phase noise realization when $\mathbf{T}$ is set as a LFT and a PPT. For comparison, we also plot the estimated phase noise realization using the CIS scheme. From Fig. 9a, we observe that the LFT matrix $\mathbf{L}$ of (5) allows only for smooth approximation of the true phase noise realization. This is because the model in (5) estimates N low-frequency components. For example, in the figure, $N = 8$ which implies eight low-frequency components are estimated. On the other hand, in Fig. 9b, we observe that when $\mathbf{T}$ is set to the PPT of (10), a piece-wise approximation of the phase noise realization is obtained. This effect arises because the interpolation matrix in (10) is a piece-wise constant interpolator. In both the figures, we observe that, using the CIS scheme, the estimated phase noise realization is a linear approximation of the true phase noise realization. As seen in the figure, for the set value of $\varrho = 0.02$ which results in a moderately-varying phase noise process, the linear approximation is a poor estimate.

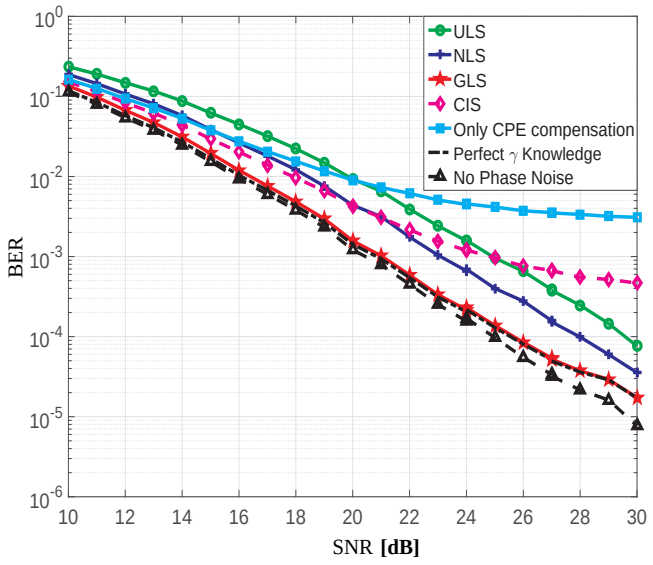

Fig. 3. Comparison of average coded BER vs. SNR for the proposed schemes with $N = 8$ and $\varrho = 0.02$. The transformation matrix used is $\mathbf{T}_{\mathrm{pc}}$ of (10).

VI. Conclusion

This paper presents scattered pilot-based phase noise estimation schemes for an OFDM radio link corrupted by phase noise. Pilot-based estimation schemes are attractive for delay sensitive wireless systems when compared to decision-feedback schemes which can incur significant computational load and, hence, delay onto the receiver. This paper builds upon earlier work wherein, using the least-squares principle, phase noise is estimated from scattered pilot subcarriers. It is shown that such an estimator suffers from amplitude and phase estimation errors which arises due to receiver noise, estimation from limited scattered pilot subcarriers and estimation using a dimensionality reduction model. We empirically show that the phase estimation error is small and the critical factor is the amplitude estimation error. To eliminate the amplitude estimation error, the least-squares estimate is enforced to satisfy the so-called phase noise spectral geometry. Numerical results demonstrate superior bit-error-rate and phase noise estimation error performance for the estimator that abides by this geometry.

Appendix A
Proof of Proposition 1

The proof follows on similar lines as in [17]. From Theorem 1, we need to prove the following:

P1. The set $\tilde{\mathbf{Q}}$ satisfies the regularity conditions, i.e., its conic hull spans the entire $\mathcal{R}^{L-1}$, where $L = N + 1$.

P2. $\mathcal{Q} \cap \mathcal{N} = \emptyset$ implies $\mathrm{cov}\,(\mathcal{Q}) \cap \mathcal{N} = \emptyset$.

We begin with P1.

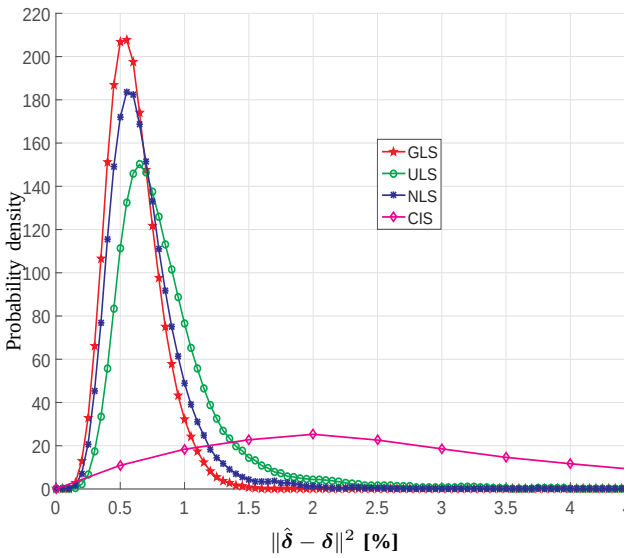

(a) SNR equal to 30-dB.

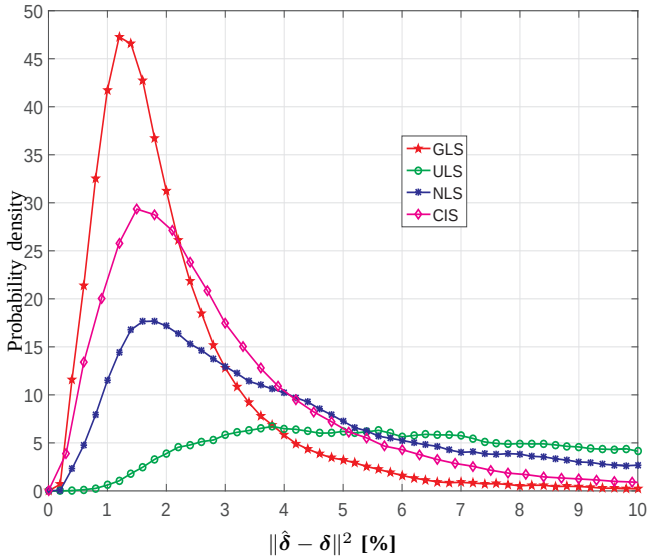

(b) SNR equal to 10-dB.

Fig. 4. Empirical PDF of $\|\hat{\boldsymbol{\delta}} - \boldsymbol{\delta}\|^2$ for the proposed schemes with $N = 8$ and $\varrho = 0.02$. The transformation matrix used is $\mathbf{T}_{\rm pc}$ of (10).

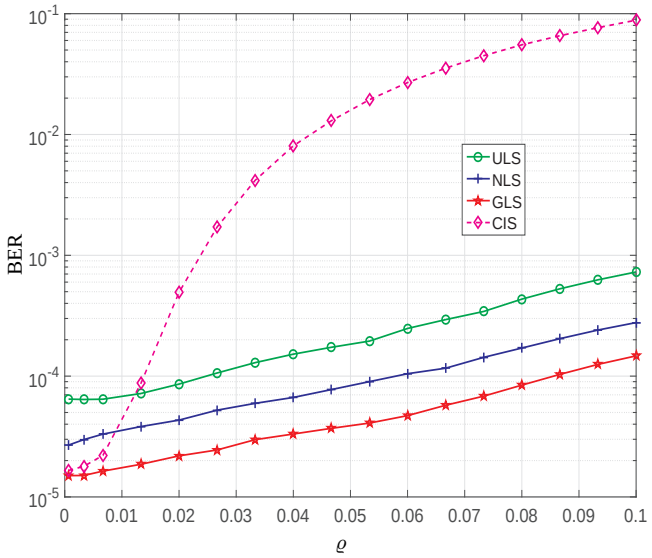

Fig. 5. Comparison of coded BER vs. ϱ for the proposed schemes with $N = 8$. The transformation matrix used is $\mathbf{T}_{\rm pc}$ of (10). The SNR is 30-dB.

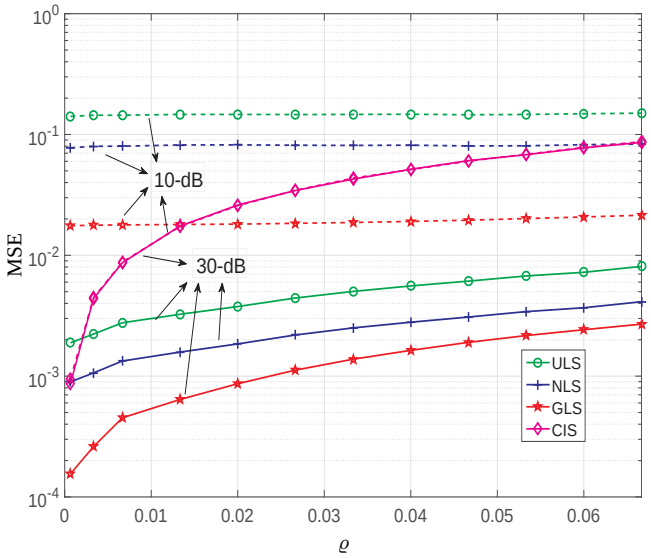

Fig. 6. Comparison of MSE of $\hat{\boldsymbol{\gamma}}$ vs. ϱ for the proposed schemes with $N = 8$. The transformation matrix used is $\mathbf{T}_{\rm pc}$ of (10).

A. Proof of P1

The set $\tilde{\mathcal{Q}}$ is described by the quadratic forms of (54) and (55), i.e.,

$$q_1(\mathbf{x}) = \mathbf{x}^\dagger \begin{pmatrix} \mathbf{I}_N & \mathbf{0} \\ \mathbf{0}^\dagger & -1 \end{pmatrix} \mathbf{x}, q_l(\mathbf{x}) = \mathbf{x}^\dagger \begin{pmatrix} \mathbf{W}_l & \mathbf{0} \\ \mathbf{0}^\dagger & 0 \end{pmatrix} \mathbf{x}, \quad (66)$$

where $\mathbf{W}_l = \tilde{\mathbf{P}}^{\rm R}_{l-1}, l = 2, 3, \ldots, \frac{N+1}{2}$ and $\mathbf{W}_l = \tilde{\mathbf{P}}^{\rm I}_{l-\frac{N+1}{2}}, l = \frac{N+1}{2}+1, \frac{N+1}{2}+2, \ldots, N$. Let $\{\tilde{\mathbf{f}}_i\}_{i=1}^N$ denote column vectors of the $N \times N$ DFT matrix $\tilde{\mathbf{F}}$. First, we note that the permutation matrix $\tilde{\mathbf{P}}_l$ is circulant and, hence, diagonalizable by $\tilde{\mathbf{F}}$. The eigenvalues of $\tilde{\mathbf{P}}_l$ are given by $\{e^{\jmath\frac{2\pi nl}{N}}\}_{n=0}^{N-1}$ and, thus, the eigenvalues of $\tilde{\mathbf{P}}_l^R$ and $\tilde{\mathbf{P}}_l^I$ are $\{\cos(\frac{2\pi nl}{N})\}_{n=0}^{N-1}$ and $\{\sin(\frac{2\pi nl}{N})\}_{n=0}^{N-1}$, respectively. We are now ready to prove the regularity condition.

Choose $\mathbf{x}_i = \begin{bmatrix} \tilde{\mathbf{f}}_i^{\rm T} & 0 \end{bmatrix}^{\rm T}, i = 1, 2, \ldots, N$ and $\mathbf{x}_{N+1} = \begin{bmatrix} \mathbf{0}^{\rm T} & \sqrt{N} \end{bmatrix}^{\rm T}$, i.e., we choose $M = N+1$ points. We note that $M > L-1$ since $L = N+1$. Making use of the eigenvalues of $\tilde{\mathbf{P}}_l^R$ and $\tilde{\mathbf{P}}_l^I$, the points $\mathbf{q}(\mathbf{x}_i)$ and, hence, the matrix $\mathbf{Q}$ of

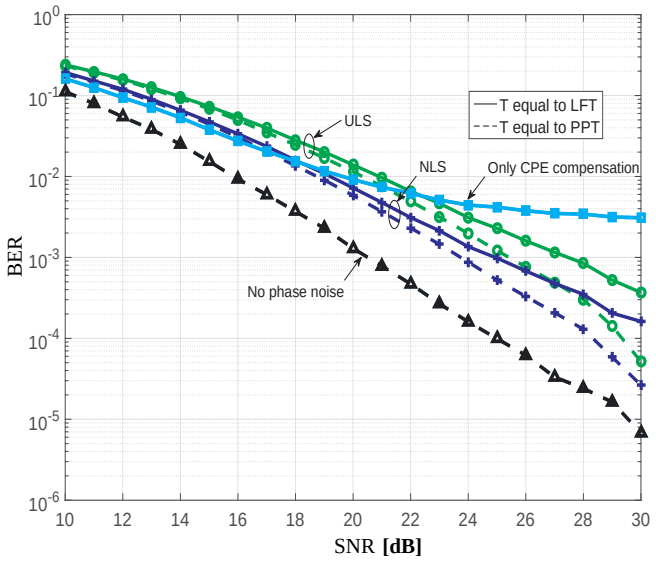

Fig. 7. Effect of $\mathbf{T}$ on average coded-BER when $\mathbf{T} = \mathbf{T}_{\rm pc}$ of (10) is compared with $\mathbf{T} = \mathbf{L}$ of (5). The value of $N = 8$ and $\varrho = 0.02$.

(19) is given by

$$\mathbf{Q} = \begin{pmatrix} 1 & 1 & 1 & \dots & 1 & -N \\ 1 & \cos(\frac{2\pi}{N}) & \cos(\frac{4\pi}{N}) & \dots & \cos(\frac{2\pi(N-1)}{N}) & 0 \\ \vdots & \vdots & \vdots & \vdots & \vdots & \vdots \\ 1 & \cos(\frac{2\pi(N-1)}{2N}) & \cos(\frac{4\pi(N-1)}{2N}) & \dots & \cos(\frac{2\pi(N-1)(N-1)}{2N}) & \vdots \\ 0 & \sin(\frac{2\pi}{N}) & \sin(\frac{4\pi}{N}) & \dots & \sin(\frac{2\pi(N-1)}{N}) & \vdots \\ \vdots & \vdots & \vdots & \vdots & \vdots & \vdots \\ 0 & \sin(\frac{2\pi(N-1)}{2N}) & \sin(\frac{4\pi(N-1)}{2N}) & \dots & \sin(\frac{2\pi(N-1)(N-1)}{2N}) & 0 \end{pmatrix}. \tag{67}$$

From (67), we note that $\mathrm{rank}\,(\mathbf{Q}) = N$ since the rows form an orthogonal basis. Choose constants $\{p_i\}_{i=1}^{M} = 1$. Then $\sum_{i=1}^{M=N+1} p_i \mathbf{q}(\mathbf{x}_i) = \mathbf{0}$ since the elements of each row sum to a value of zero. This completes the proof.

B. Proof of P2

The set $\mathcal{Q}$ is defined in (12) and described by the quadratic forms $q_l(\mathbf{x}), l = 0, 1, \dots N$, where $q_l(\mathbf{x}), l > 0$ is given in (66). The quadratic form $q_0(\mathbf{x})$ takes the form

$$q_0(\mathbf{x}) = \mathbf{x}^\dagger \begin{pmatrix} \mathbf{M} & \mathbf{b} \\ \mathbf{b}^\dagger & -\tau \end{pmatrix} \mathbf{x}. \tag{68}$$

Consider the set

$$\mathcal{Q}_N = \left\{ \Big(q_0(\mathbf{x}),\ q_1(\mathbf{x}), \dots, q_N(\mathbf{x})\Big)^{\rm T} : ||\mathbf{x}||_2 = 1, \mathbf{x} \in \mathcal{C}^{N+1} \right\}. \tag{69}$$

It is related to $\mathcal{Q}$ by [37], [38]

$$\mathcal{Q} = \left\{ t\mathbf{y} \;\middle|\; t \geq 0,\ \mathbf{y} \in \mathcal{Q}_N \right\}. \tag{70}$$

Let $\mathrm{cov}\,(\mathcal{Q}_N)$ denote the convex hull of $\mathcal{Q}_N$. We define

$$\mathrm{con}\,(\mathcal{Q}) = \left\{ t\mathbf{y} \;\middle|\; t \geq 0,\ \mathbf{y} \in \mathrm{cov}\,(\mathcal{Q}_N) \right\}. \tag{71}$$

First, we observe that $\mathcal{Q} \subseteq \mathrm{con}\,(\mathcal{Q})$. Secondly, $\mathrm{con}\,(\mathcal{Q})$ is a convex set since it is defined in terms of the convex set $\mathrm{cov}\,(\mathcal{Q}_N)$. We, thus, have

$$\mathrm{cov}\,(\mathcal{Q}) \subseteq \mathrm{con}\,(\mathcal{Q}), \tag{72}$$

since $\mathrm{cov}\,(\mathcal{Q})$ is the convex hull of $\mathcal{Q}$ and by definition is the smallest convex set enclosing $\mathcal{Q}$. With these facts in place, we have the following relation:

R1. $\mathcal{Q} \cap \mathcal{N} = \emptyset \equiv \mathcal{Q}_N \cap \mathcal{N} = \emptyset$.

R2. $\mathrm{cov}\,(\mathcal{Q}_N) \cap \mathcal{N} = \emptyset \implies \mathrm{con}\,(\mathcal{Q}) \cap \mathcal{N} = \emptyset \implies \mathrm{cov}\,(\mathcal{Q}) \cap \mathcal{N} = \emptyset$,

where $\equiv$ denotes equivalence and $\implies$ denotes implication. The equivalence in R1 follows from (69) and (70). The implication in R2 follows from (71). We, thus, see that if $\mathcal{Q}_N \cap \mathcal{N} = \emptyset \implies \mathrm{cov}\,(\mathcal{Q}_N) \cap \mathcal{N} = \emptyset$ then, after combining R1 and R2, we have the required result. We now show that this is indeed the case.

***Remark* 4.** *For unit-norm* $\mathbf{x}$, $q_1(\mathbf{x}) = 0$ *only at* $\mathbf{x} = \left[\sqrt{0.5}\tilde{\mathbf{x}}^{\rm T}\sqrt{0.5}z\right]^{\rm T}$, *where* $\|\tilde{\mathbf{x}}\|_2 = 1$ *and* $|z| = 1$.

Proposition 2. *For unit-norm* $\mathbf{x}$, $q_l(\mathbf{x}) = 0$ *for all* $l > 1$ *at*

$$\mathbf{x} = \left[\sqrt{a}\tilde{\mathbf{x}}^{\rm T}\sqrt{b}z\right]^{\rm T}, \tilde{\mathbf{x}} = \mathbf{F}\Sigma\tilde{\mathbf{v}}, \tilde{\mathbf{v}}^{\rm T}\tilde{\mathbf{v}} = 1, |z| = 1, \tag{73}$$

where $\tilde{\mathbf{v}}_i = \frac{1}{\sqrt{N}}$, $a \geq 0, b \geq 0$, $a + b = 1$ *and* Σ *can be any unitary-diagonal matrix.*

Proof: Write $\mathbf{x} = \left[\sqrt{a}\tilde{\mathbf{x}}^{\rm T}\sqrt{b}z\right]^{\rm T}$. Since $\mathbf{x}$ should be of unit-norm, we have $\|\tilde{\mathbf{x}}\|_2 = 1$, $a \geq 0, b \geq 0$, $a + b = 1$ and $|z| = 1$. Using (66), the condition $q_l(\mathbf{x}) = 0, l > 1$ results in

$$\tilde{\mathbf{x}}^\dagger \mathbf{W}_l \tilde{\mathbf{x}} = 0 \implies \tilde{\mathbf{x}}^\dagger \tilde{\mathbf{F}} \tilde{\mathbf{D}}_l \tilde{\mathbf{F}}^\dagger \tilde{\mathbf{x}} = 0 \implies \mathbf{y}^\dagger \tilde{\mathbf{D}}_l \mathbf{y} = \mathbf{d}_l^{\rm T}\mathbf{v} = 0,$$

where $\mathbf{y} = \tilde{\mathbf{F}}^\dagger\tilde{\mathbf{x}}$ with components denoted by $\mathbf{y}_i$ and $\mathbf{v} = \left[|\mathbf{y}_0|^2\ |\mathbf{y}_1|^2 \dots |\mathbf{y}_{N-1}|^2\right]^{\rm T}$. In the above equation, we used the fact that $\mathbf{W}_l$ is diagonalizable with the DFT matrix whose eigenvalues are contained in the diagonal matrix $\tilde{\mathbf{D}}_l$ and in the vector $\mathbf{d}_i$. Combining above equation for all $l \geq 2$, we get

$$\begin{pmatrix} 1 & \cos(\frac{2\pi}{N}) & \cos(\frac{4\pi}{N}) & \dots & \cos(\frac{2\pi(N-1)}{N}) \\ \vdots & \vdots & \vdots & \vdots & \vdots \\ 1 & \cos(\frac{2\pi(N-1)}{2N}) & \cos(\frac{4\pi(N-1)}{2N}) & \dots & \cos(\frac{2\pi(N-1)(N-1)}{2N}) \\ 0 & \sin(\frac{2\pi}{N}) & \sin(\frac{4\pi}{N}) & \dots & \sin(\frac{2\pi(N-1)}{N}) \\ \vdots & \vdots & \vdots & \vdots & \vdots \\ 0 & \sin(\frac{2\pi(N-1)}{2N}) & \sin(\frac{4\pi(N-1)}{2N}) & \dots & \sin(\frac{2\pi(N-1)(N-1)}{2N}) \end{pmatrix} \mathbf{v} = \mathbf{0}, \tag{74}$$

where we require that $\mathbf{v} \succeq 0$ and $\|\mathbf{v}\|_1 = 1$ because $\|\tilde{\mathbf{x}}\|_2 = 1$. It can be easily seen that the above matrix has a non-zero null space of rank equal to one. The vector describing this space (and satisfying $\mathbf{v} \succeq 0$, $\|\mathbf{v}\|_1 = 1$) is given by

$$\mathbf{v} = \frac{1}{N}\mathbf{1}, \tag{75}$$

where $\mathbf{1}$ denotes N-dimensional vector of ones. Define $\tilde{\mathbf{v}}$ as the vector with elements $\tilde{\mathbf{v}}_i = \sqrt{\mathbf{v}_i}$. Thus, at $\tilde{\mathbf{x}} = \tilde{\mathbf{F}}\Sigma\tilde{\mathbf{v}}$, where Σ can be any unitary-diagonal matrix, $\tilde{\mathbf{x}}^\dagger \mathbf{W}_l \tilde{\mathbf{x}} = 0$, for all $l \geq 2$. ■

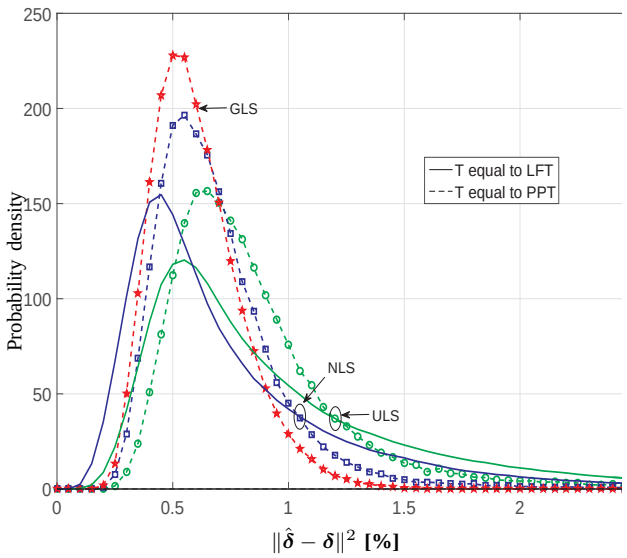

(a) SNR equal to 30-dB. Observe that the PDF has thicker tails when $\mathbf{T}$ is set to LFT, thus, exhibiting higher BER in Fig. 7 at 30-dB SNR.

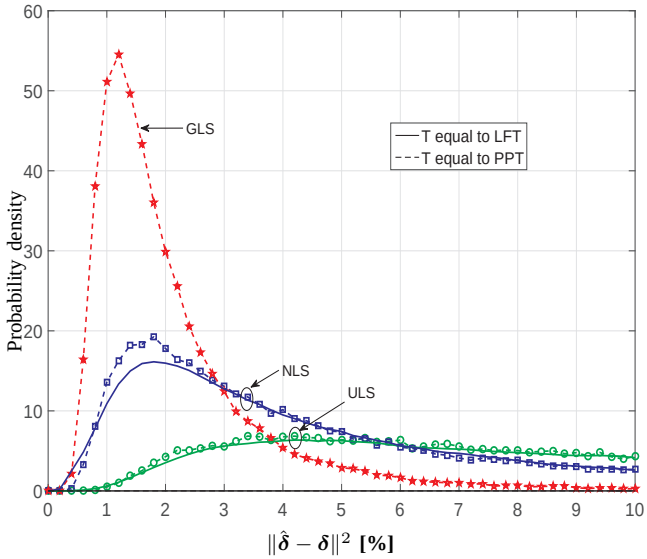

(b) SNR equal to 10-dB. Observe that for ULS and NLS, there is no dependence of the PDF tails on the choice of $\mathbf{T}$, thus, exhibiting similar BER values in Fig. 7 at 10-dB SNR.

Fig. 8. Effect of $\mathbf{T}$ on the empirical PDF of $\|\hat{\boldsymbol{\delta}} - \boldsymbol{\delta}\|^2$ for the proposed schemes. $\mathbf{T}_{\rm pc}$ of (10) is used as the PPT and $\mathbf{L}$ of (5) is the LFT. The number of estimated components is $N = 8$. The value of $\varrho = 0.02$. The GLS is also plotted for comparison. It is always implemented with $\mathbf{T}$ set to a PPT.

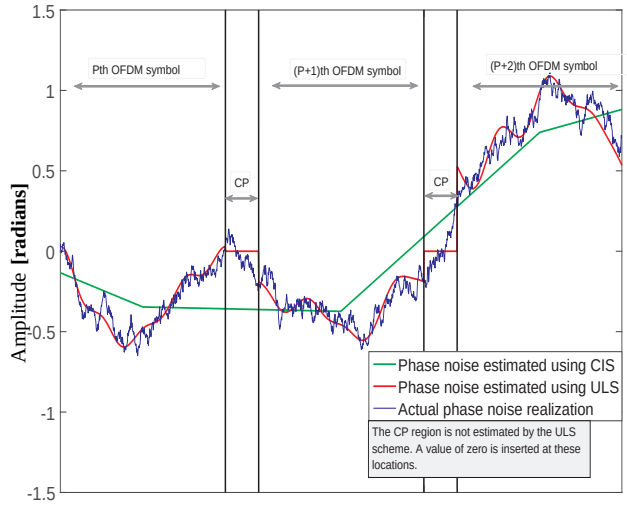

(a) $\mathbf{T}$ set to LFT of (5).

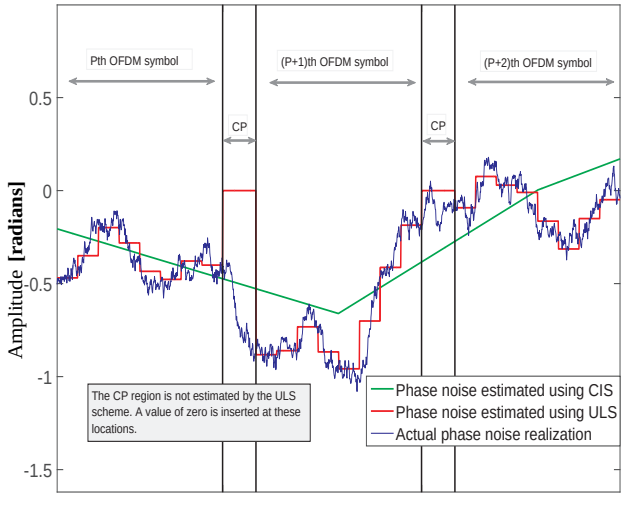

(b) $\mathbf{T}$ set to PPT of (10).

Fig. 9. Comparison of the estimated phase noise realization with the actual phase noise realization. The value of $N = 8$ and $\varrho = 0.02$ with 30-dB SNR.

Proposition 3. *For any $a \geq 0$ and $b \geq 0$, such that $a > b$ and $a + b = 1$, we have*

$$\begin{aligned} &\text{infimum}\left(\tilde{\mathbf{x}}^\dagger \mathbf{A}\tilde{\mathbf{x}} + 2\text{Real}\left(\tilde{\mathbf{x}}^\dagger \mathbf{c}\right)\right) \leq \\ &\text{infimum}\left(\tilde{\mathbf{x}}^\dagger \mathbf{A}\tilde{\mathbf{x}} + \sqrt{\frac{\text{b}}{\text{a}}} 2\text{Real}\left(\tilde{\mathbf{x}}^\dagger \mathbf{c}\right)\right), \end{aligned} \tag{76}$$

where $\mathbf{A} \succ 0$, $\mathbf{c}$ is any complex vector and the infimum is taken over all $\tilde{\mathbf{x}}$ satisfying (73)*.*

Proof: First, we note there exists an $\tilde{\mathbf{x}}$ satisfying (73) such that $\text{Real}\left(\tilde{\mathbf{x}}^\dagger \mathbf{c}\right) \leq 0$. For example, from (73), the components of the row vector $\tilde{\mathbf{v}}^\dagger \Sigma^\dagger$ take the form $\frac{e^{-\jmath\phi_l}}{\sqrt{N}}$, where $e^{\jmath\phi_l}$ are the diagonal values of diagonal Σ matrix. Since Σ can be any unitary-diagonal matrix, set $\phi_l = \angle\left(\tilde{\mathbf{F}}^\dagger \mathbf{c}\right)_l - \pi$, where $\angle x$ denotes angle of the complex number x. Thus, $\text{Real}\left(\tilde{\mathbf{v}}^\dagger \Sigma^\dagger \tilde{\mathbf{F}}^\dagger \mathbf{c}\right) = -\|\tilde{\mathbf{F}}^\dagger \mathbf{c}\|_1 \leq 0$. Thus, we have

$$\text{infimum}\left(\tilde{\mathbf{x}}^\dagger \mathbf{A}\tilde{\mathbf{x}} + 2\text{Real}\left(\tilde{\mathbf{x}}^\dagger \mathbf{c}\right)\right) = \eta - \epsilon \tag{77}$$

$$\text{infimum}\left(\tilde{\mathbf{x}}^\dagger \mathbf{A}\tilde{\mathbf{x}} + \sqrt{\frac{\text{b}}{\text{a}}} 2\text{Real}\left(\tilde{\mathbf{x}}^\dagger \mathbf{c}\right)\right) = \eta - \sqrt{\frac{b}{a}}\epsilon, \tag{78}$$

where $\epsilon \geq 0$ and η is the minimum eigenvalue of $\mathbf{A}$. The

result now follows since $a > b$. ■

Let $\mathrm{con}\left(\mathcal{Q}_N\right)$ denote the conic hull of $\mathcal{Q}_N$. We now have the following proposition:

Proposition 4. *Let* $\tau \leq \mathrm{infimum}\left(\tilde{\mathbf{x}}^\dagger \mathbf{M}\tilde{\mathbf{x}} + 2\mathrm{Real}\left(\tilde{\mathbf{x}}^\dagger \mathbf{b}z\right)\right)$. *The point* $[0, 1, 0 \ldots 0]^{\mathrm{T}} \notin \mathrm{con}\left(\mathcal{Q}_N\right)$.

Proof: If $[0, 1, 0 \ldots 0]^{\mathrm{T}} \in \mathrm{con}\left(\mathcal{Q}_N\right)$ then there must exist $[0, t, 0 \ldots 0]^{\mathrm{T}} \in \mathcal{Q}_N$ for some $t > 0$ [37]. We show that this is impossible. From Proposition 2, we have $q_l(\mathbf{x}) = 0, l > 1$ for $\mathbf{x}$ of (73). At such an $\mathbf{x}$, $q_1(\mathbf{x}) = a - b$ and, since we require $[0, t, 0 \ldots 0]^{\mathrm{T}} \in \left(\mathcal{Q}_N\right)$ for $t > 0$, we require $a > b$. Now, the quadratic form $q_0(\mathbf{x})$ of (68), for $\mathbf{x}$ of (73), takes the form

$$q_0(\mathbf{x}) = a\left[\tilde{\mathbf{x}}^\dagger \mathbf{M}\tilde{\mathbf{x}} + \sqrt{\frac{b}{a}} 2\mathrm{Real}\left(\tilde{\mathbf{x}}^\dagger \mathbf{b}z\right)\right] - b\tau > 0, \quad (79)$$

where the inequality results after applying Proposition 3 and the assumption that $\tau \leq \mathrm{infimum}\left(\tilde{\mathbf{x}}^\dagger \mathbf{M}\tilde{\mathbf{x}} + 2\mathrm{Real}\left(\tilde{\mathbf{x}}^\dagger \mathbf{b}z\right)\right)$. Using (79), we see that $[0, t, 0 \ldots 0]^{\mathrm{T}} \notin \mathcal{Q}_N$ for $t > 0$. ■

The proof of P2 is now complete with the following proposition and after combining the relations R1 and R2.

Proposition 5. $\mathcal{Q}_N \cap \mathcal{N} = \emptyset \implies \mathrm{cov}\left(\mathcal{Q}_N\right) \cap \mathcal{N} = \emptyset$.

Proof: The condition $\mathcal{Q}_N \cap \mathcal{N} = \emptyset$ implies $q_0(\mathbf{x}) \geq 0$ and $q_l(\mathbf{x}) = 0, l \geq 1$. From Remark 4 and Proposition 2, we have $q_l(\mathbf{x}) = 0$ for $l \geq 1$ only at $\mathbf{x} = \left[\sqrt{0.5}\tilde{\mathbf{x}}^{\mathrm{T}} \sqrt{0.5}z\right]^{\mathrm{T}}$, where $\tilde{\mathbf{x}}$ and z satisfy (73). At such an $\mathbf{x}$, $q_0(\mathbf{x}) \geq 0$ implies

$$0.5\left[\tilde{\mathbf{x}}^\dagger \mathbf{M}\tilde{\mathbf{x}} + 2\mathrm{Real}\left(\tilde{\mathbf{x}}^\dagger \mathbf{b}z\right) - \tau\right] \geq 0 \quad (80)$$

$$\implies \tau \leq \tilde{\mathbf{x}}^\dagger \mathbf{M}\tilde{\mathbf{x}} + 2\mathrm{Real}\left(\tilde{\mathbf{x}}^\dagger \mathbf{b}z\right), \quad (81)$$

$$\implies \tau \leq \mathrm{infimum}\left(\tilde{\mathbf{x}}^\dagger \mathbf{M}\tilde{\mathbf{x}} + 2\mathrm{Real}\left(\tilde{\mathbf{x}}^\dagger \mathbf{b}z\right)\right), \quad (82)$$

where the infimum is taken over all values of $\tilde{\mathbf{x}}$ and z satisfying (73). Thus, after using Proposition 4, we have that $[0, 1, 0 \ldots 0]^{\mathrm{T}} \notin \mathrm{con}\left(\mathcal{Q}_N\right)$. This implies that the *origin is boundary point* of $\mathrm{con}\left(\mathcal{Q}_N\right)$. A necessary and sufficient condition for origin to be a boundary point is existence of a point that does not belong to $\mathrm{con}\left(\mathcal{Q}_N\right)$ [37]. Thus, $\mathcal{Q}_N \cap \mathcal{N} = \emptyset \implies \mathrm{con}\left(\mathcal{Q}_N\right) \cap \mathcal{N} = \emptyset \implies \mathrm{cov}\left(\mathcal{Q}_N\right) \cap \mathcal{N} = \emptyset$. ■

Pramod Mathecken received his M.Sc. and D.Sc. degrees in signal processing from Aalto University, Finland in 2011 and 2016, respectively. His research interest is in the field of signal processing and wireless communications.

Taneli Riihonen (S'06–M'14) received the D.Sc. degree in electrical engineering (with distinction) from Aalto University, Finland, in August 2014. He has held various research positions at the Department of Signal Processing and Acoustics, Aalto University School of Electrical Engineering since September 2005, being currently appointed as a Research Fellow. He was a Visiting Associate Research Scientist and an Adjunct Assistant Professor at Columbia University in the City of New York, USA, from November 2014 through December 2015. He has been praised nine times as a distinguished reviewer for various IEEE journals and is serving as an Editor for IEEE COMMUNICATIONS LETTERS since October 2014. He received the Finnish technical sector's award for the best doctoral dissertation of the year in Finland within all engineering sciences. His research activity is focused on physical-layer OFDM(A), multiantenna, relaying and full-duplex wireless techniques with current interest in the evolution of 5G systems.

Stefan Werner (SM'07) received the M.Sc. degree in electrical engineering from the Royal Institute of Technology (KTH), Stockholm, Sweden, in 1998 and the D.Sc. degree with honors in electrical engineering from the Signal Processing Laboratory, Helsinki University of Technology (TKK), Espoo, Finland, in 2002. He is currently Professor at the Department of Electronic Systems at the Norwegian University of Science and Technology (NTNU). He is also an Adjunct Professor with Aalto University in Finland, and an Adjunct Senior Research Fellow with the Institute for Telecommunications Research, University of South Australia. He was holding an Academy Research Fellowship funded by the Academy of Finland from 2009 to 2014. His research interests include adaptive and statistical signal processing, signal processing for communications, and smart electric power grids. Dr. Werner is a member of the editorial board for the EURASIP journal of Signal Processing.

Risto Wichman received his M.Sc. and D.Sc. (Tech) degrees in digital signal processing from Tampere University of Technology, Tampere, Finland, in 1990 and 1995, respectively. From 1995 to 2001, he worked at Nokia Research Center as a senior research engineer. In 2002, he joined Department of Signal Processing and Acoustics, Aalto University School of Electrical Engineering, Finland, where he is a full professor since 2008. His research interests include signal processing techniques for wireless communication systems.

REFERENCES

[1] G. Fettweis, M. Löhning, D. Petrovic, M. Windisch, P. Zillmann, and W. Rave, "Dirty RF: A new paradigm," *International Journal of Wireless Information Networks*, vol. 14, no. 2, pp. 133–148, June 2007.

[2] R. Enrico, *Phase noise and Frequency Stability in Oscillators*. Cambridge University Press, 2009.

[3] J. Stott, "The effects of phase noise in COFDM," *EBU Technical Review*, Summer 1998.

[4] T. Pollet, M. Van Bladel, and M. Moeneclaey, "BER sensitivity of OFDM systems to carrier frequency offset and Wiener phase noise," *IEEE Trans. Commun.*, vol. 43, no. 234, pp. 191–193, February/April 1995.

[5] J. Montojo and L. Milstein, "Effects of imperfections on the performance of OFDM systems," *IEEE Trans. Commun.*, vol. 57, no. 7, pp. 2060–2070, July 2009.

[6] P. Mathecken, T. Riihonen, N. Tchamov, S. Werner, M. Valkama, and R. Wichman, "Characterization of OFDM radio link under PLL-based oscillator phase noise and multipath fading channel," *IEEE Trans. Commun.*, vol. 60, no. 6, pp. 1479–1485, June 2012.

[7] P. Mathecken, T. Riihonen, S. Werner, and R. Wichman, "Performance analysis of OFDM with Wiener phase noise and frequency selective fading channel," *IEEE Trans. Commun.*, vol. 59, no. 5, pp. 1321–1331, May 2011.

[8] F. Gregorio, J. Cousseau, S. Werner, T. Riihonen, and R. Wichman, "EVM analysis for broadband OFDM direct-conversion transmitters," *IEEE Trans. Veh. Technol.*, vol. 62, no. 7, pp. 3443–3451, September 2013.

[9] A. Demir, "Phase noise and timing jitter in oscillators with colored-noise sources," *IEEE Transactions on Circuits and Systems I: Fundamental Theory and Applications*, vol. 49, no. 12, pp. 1782–1791, December 2002.

[10] L. Anttila, "Digital front-end signal processing with widely-linear signal models in radio devices," PhD, Tampere University of Technology, Department of Communications Engineering, 2011.

[11] D. D. Lin, R. Pacheco, T. J. Lim, and D. Hatzinakos, "Joint estimation of channel response, frequency offset, and phase noise in OFDM," *IEEE Trans. Signal Process.*, vol. 54, no. 9, pp. 3542–3554, 2006.

[12] P. Rabiei, W. Namgoong, and N. Al-Dhahir, "A non-iterative technique for phase noise ICI mitigation in packet-based OFDM systems," *IEEE Trans. Signal Process.*, vol. 58, no. 11, pp. 5945–5950, November 2010.

[13] F. Septier, Y. Delignon, A. Menhaj-Rivenq, and C. Garnier, "Monte carlo methods for channel, phase noise, and frequency offset estimation with unknown noise variances in OFDM systems," *IEEE Trans. Signal Process.*, vol. 56, no. 8, pp. 3613–3626, August 2008.

[14] F. Munier, T. Eriksson, and A. Svensson, "An ICI reduction scheme for OFDM system with phase noise over fading channels," *IEEE Trans. Commun.*, vol. 56, no. 7, pp. 1119–1126, July 2008.

[15] R. Carvajal, J. Aguero, B. Godoy, and G. Goodwin, "EM-based maximum-likelihood channel estimation in multicarrier systems with phase distortion," *IEEE Trans. Veh. Technol.*, vol. 62, no. 1, pp. 152–160, January 2013.

[16] O. H. Salim, A. A. Nasir, H. Mehrpouyan, W. Xiang, S. Durrani, and R. A. Kennedy, "Channel, phase noise, and frequency offset in OFDM systems: Joint estimation, data detection, and hybrid Cramer-Rao lower bound," *IEEE Trans. Commun.*, vol. 62, no. 9, pp. 3311–3325, September 2014.

[17] P. Mathecken, T. Riihonen, S. Werner, and R. Wichman, "Phase noise estimation in OFDM: Utilizing its associated spectral geometry," *IEEE Trans. Signal Process.*, vol. 64, no. 8, pp. 1999–2012, 2016.

[18] V. Syrjälä and M. Valkama, "Iterative receiver signal processing for joint mitigation of transmitter and receiver phase noise in OFDM-based cognitive radio link," in *Proc. International Conference on Cognitive Radio Oriented Wireless Networks*, June 2012.

[19] ——, "Receiver DSP for OFDM systems impaired by transmitter and receiver phase noise," in *Proc. IEEE International Conference on Communications (ICC)*, June 2011, pp. 1–6.

[20] D. Petrovic, W. Rave, and G. Fettweis, "Effects of phase noise on OFDM systems with and without PLL: Characterization and compensation," *IEEE Trans. Commun.*, vol. 55, no. 8, pp. 1607–1616, August 2007.

[21] S. Wu, P. Liu, and Y. Bar-Ness, "Phase noise estimation and mitigation for OFDM systems," *IEEE Trans. Wireless Commun.*, vol. 5, no. 12, pp. 3616–3625, December 2006.

[22] V. Syrjälä, M. Valkama, N. Tchamov, and J. Rinne, "Phase noise modelling and mitigation techniques in OFDM communications systems," in *Proc. Wireless Telecommunications Symposium*, April 2009, pp. 1–7.

[23] R. Casas, S. Biracree, and A. Youtz, "Time domain phase noise correction for OFDM signals," *IEEE Transactions on Broadcasting*, vol. 48, no. 3, pp. 230–236, 2002.

[24] D. Yee, J. P. Reilly, and T. Kirubarajan, "A blind sequential monte carlo detector for OFDM systems in the presence of phase noise, multipath fading, and channel order uncertainty," *IEEE Trans. Signal Process.*, vol. 55, no. 9, pp. 4581–4598, 2007.

[25] D. D. Lin and T. J. Lim, "The variational inference approach to joint data detection and phase noise estimation in OFDM," *IEEE Trans. Signal Process.*, vol. 55, no. 5, pp. 1862–1874, 2007.

[26] S. Särkkä, *Bayesian Filtering and Smoothing*. Cambridge University Press, 2013.

[27] W. Songping and Y. Bar-Ness, "OFDM systems in the presence of phase noise: Consequences and solutions," *IEEE Trans. Commun.*, vol. 52, no. 11, pp. 1988–1996, November 2004.

[28] K. Nikitopoulos and A. Polydoros, "Phase-impairment effects and compensation algorithms for OFDM systems," *IEEE Trans. Commun.*, vol. 53, no. 4, pp. 698–707, April 2005.

[29] K. Kim, Q. Zou, H. J. Choi, and A. Sayed, "An efficient carrier phase synchronization technique for high-order M-QAM-OFDM," *IEEE Trans. Signal Process.*, vol. 56, no. 8, pp. 3789–3794, August 2008.

[30] M. O. Pun, M. Morelli, and C. C. J. Kuo, *Multi-carrier techniques for broadband wireless communications*. Imperial College Press, 2007.

[31] S. Boyd and L. Vandenberghe, *Convex Optimization*. Cambridge University Press, 2004.

[32] U. T. Jonsson, *A Lecture on the S-procedure*. Division of Optimization and System Theory, Royal Institute of Technology (KTH), 2006.

[33] A. Ben-Tal and A. Nemirovski, *Lectures on modern convex optimization: Analysis, algorithms, and engineering applications*. SIAM, 2001.

[34] Y. Nesterov and A. Nemirovski, *Interior-Point Polynomial Algorithms in Convex Programming*. SIAM, 1994.

[35] M. C. Grant and S. P. Boyd, *Recent Advances in Learning and Control*. Springer, 2008, ch. Graph Implementations for Nonsmooth Convex Programs, pp. 95–110.

[36] M. C. Grant, S. P. Boyd, and Y. Ye, "CVX: Matlab software for disciplined convex programming," *Available at http://cvxr.com/cvx*.

[37] L. L. Dines, "On the mapping of N quadratic forms," *Bulletin of the American Mathematical Society*, vol. 48, no. 6, pp. 467–471, 1942.

[38] L. Brickman, "On the field of values of a matrix," *Proceedings of the American Mathematical Society*, vol. 12, no. 1, pp. 61–66, 1961.